Received: 31 December 2021 | Revised: 10 February 2022 | Accepted: 19 February 2022

DOI: 10.1002/smm2.1103

REVIEW

SmartMat Open Access WILEY

Recent progress in the all-solid-state flexible supercapacitors

Yongrui Yang[1] | Tao Zhu[1] | Lening Shen[1] | Yanghe Liu[1] | Dong Zhang[2] | Bowen Zheng[3] | Keven Gong[4] | Jie Zheng[2] | Xiong Gong[1,2]

[1]School of Polymer Science and Polymer Engineering, The University of Akron, Akron, Ohio, USA

[2]Department of Chemical, Biomolecular and Corrosion Engineering, The University of Akron, Akron, Ohio, USA

[3]Copley High School, Copley, Ohio, USA

[4]Western Reserve Academy, Hudson, Ohio, USA

Correspondence
Xiong Gong, School of Polymer Science and Polymer Engineering, The University of Akron, Akron, OH 44325, USA.
Email: xgong@uakron.edu

Funding information
National Science Foundation, Grant/Award Number: ECCS/EPMD1903303

Abstract

In the past few years, supercapacitors (SCs) have attracted great attention in both academic and industrial sectors due to their high energy storage efficiency, reliable stability, and eco-friendly process. Flexible solid-state SCs as one of the ongoing focuses for the development of wearable and portable electronics have become the most promising energy storage devices for the smart power system due to their high power density, fast electrochemical response, high efficiency on the charge-discharge process, and excellent electrochemical stability. In this study, the recent progress in the electrodes and electrolytes used for approaching high-performance of the all-solid-state flexible SCs is reviewed. We first introduce basic operational principles of various SCs. And then we overview the electrode materials including carbon materials, conducting polymers, transition metal oxides/chalcogenides/nitrides, MXenes, metal-organic frameworks, covalent-organic frameworks, and the polymer-based solid-state electrolytes in different systems. Afterward, we summarize recent progress in the development of the all-solid-state flexible SCs and outlook for future research directions.

KEYWORDS

electrode materials, electrolyte materials, flexible supercapacitors, solid-state supercapacitors

1 | INTRODUCTION

With the decreased availability of fossil fuel and rapid development of the global economy, eco-friendly, renewable, and sustainable energy sources and related technologies present an important role in our daily life.[1–3] In the past few years, electrical energy storage (EES) devices and systems have attracted more and more attention due to their high energy storage efficiency.[4–6] Electrochemical batteries, capacitors, and supercapacitors (SCs) are three different EES devices. Figure 1 displays the Ragone plot to describe the energy density and power density of various EES devices.[7] The capacitors possess very high power density but quite low energy density. In contrast, electrochemical batteries have high energy density but relatively low power density.[7] SCs can bridge the electrochemical batteries and capacitors with the preponderance in both energy density and power density.

The main differences between SCs and electrochemical batteries are their different operational mechanisms in

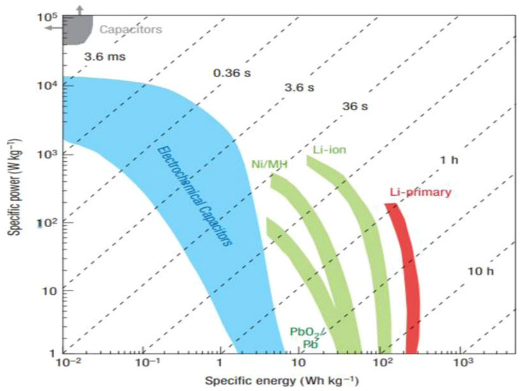

FIGURE 1 Ragone plot of various electrical energy storage devices. Reproduced with permission: Copyright 2008, Springer Nature[7]

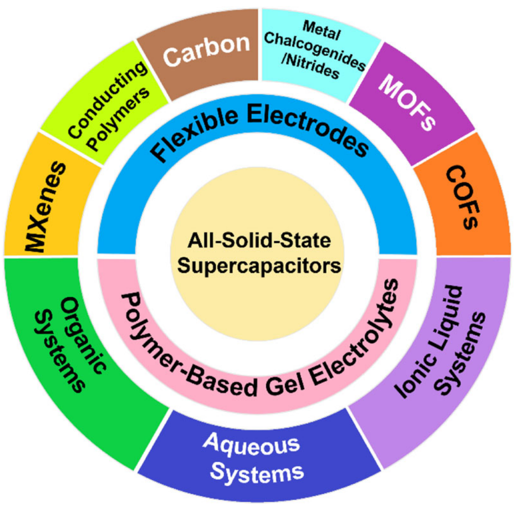

SCHEME 1 The classification of electrode and electrolyte materials for flexible all-solid-state supercapacitors

storing charges. In electrochemical batteries, the charges are stored in the bulk electrodes, which provides a higher energy density, whereas, in SCs, the charges are stored in the interface between the electrodes and the electrolytes, resulting in a higher power density.[8–11]

As the potential candidates for the next-generation flexible energy storage devices, SCs have attracted abundant attention in both academic and industrial sectors.[12] Different from commercial SCs where the liquid electrolytes are sealed by clumsy crusts, in the flexible solid-state SCs, polyelectrolytes serve as both electrolytes and separators.[13,14] Moreover, the solid metallic crust was required to seal the traditional commercial SCs for preventing the leakage of the toxic organic liquid electrolytes, restricting their applications as wearable and flexible electronics.[15,16] Whereas, the flexible solid-state SCs are fabricated by a piece of a polymer gel as both electrolytes and separators, which is sandwiched by two flexible electrodes. The ongoing directions are to develop the electrodes with high pseudocapacitive properties and long-lifetime and the electrolytes with both super-flexibility and excellent ionic conductivity.[15,17–19]

In this study, we start with an introduction of SCs and then describe the operational principles of SCs. Afterward, the progress in the development of both electrodes and electrolytes for the flexible SCs is overviewed as illustrated in Scheme 1. In the last, we present a summary and outlook of the flexible SCs.

2 | OPERATIONAL PRINCIPLES OF SCS

The basic operation principles of three different SCs will be described in this section.

2.1 | Electric double-layer capacitors

Figure 2 presents the three models which illustrate the operational principles of the electric double-layer capacitors (EDLCs).[20] The basic operational principles of the EDLC in storing the energy is originated from the ionic electrostatic adsorption and desorption processes at the interface between the electrodes and the electrolytes. The Helmholtz model is the simplest one that describes such behaviors, as proposed by Helmholtz in 1853.[21] As shown in Figure 2A, AS the electrode surface is polarized, the ions with the opposite charge within the electrolytes will drift to the interface between the electrodes and the electrolytes, and then form a several-nanometer condensed layer. The capacitance (C_H) of this double-layer is described by following equation[20]:

$$C_{\mathrm{H}} = \varepsilon_0 \varepsilon_r s/d, \quad (1)$$

where ε_0 is the vacuum permittivity (8.854×10^{-12} F/m); ε_r is the relative permittivity of the dielectric electrolyte; d is the thickness of the electric double layer; and s is the area of the interface between the electrodes and the electrolytes, respectively. In the Helmholtz model, d is typically within the nanometer scale. Thus, the electrodes with a large surface area will generate a larger total capacitance compared to the traditional parallel plate capacitors. Based on the Helmholtz model, Gouy–Chapman further established another model, as indicated in Figure 2B. In the Gouy–Chapman model, the ions diffusion behaviors and the interaction between the electrodes and solvents were taken into account.[22] In addition, the Gouy–Chapman model indicated that the

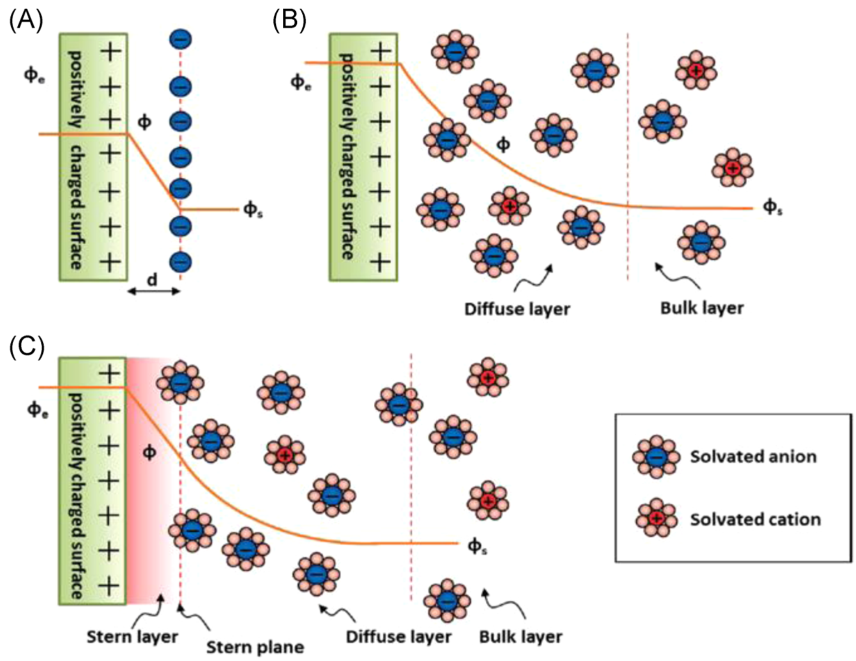

FIGURE 2 (A) Helmholtz, (B) Gouy–Chapman, and (C) Stern models of the electrical double-layer formed at a positively charged electrode in an aqueous electrolyte. Reproduced with permission: Copyright 2014, John Wiley and Sons[20]

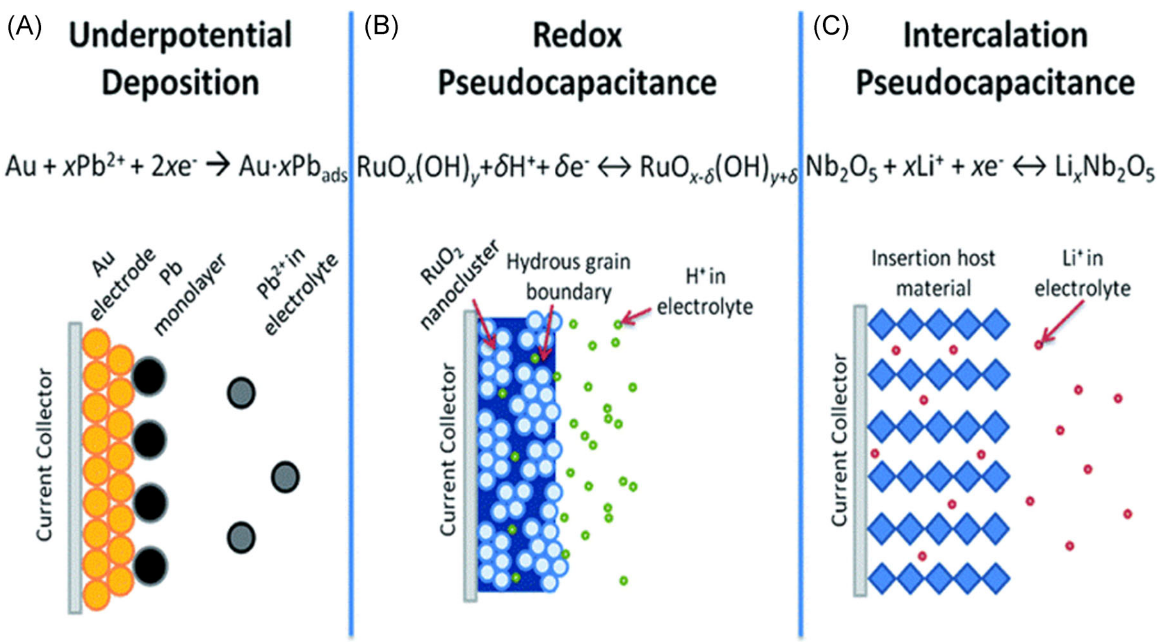

FIGURE 3 Different types of reversible redox mechanisms that give rise to pseudocapacitance: (A) underpotential deposition, (B) redox pseudocapacitance, and (C) intercalation pseudocapacitance. Reproduced with permission: Copyright 2013, Royal Society of Chemistry[24]

electrical potential of the diffusion layer was exponentially decreased from the electrode (Φ_e) to the bulk solution (Φ_s). Stern combined the above two models and presented another model termed as Stern model, as indicated in Figure 2C. The Stern model was suitable for the highly charged double-layer,[23] where the Stern plane shows the minimum distance between the electrode surface and ions.

2.2 | Pseudocapacitors

Figure 3 displays the operational principles of pseudocapacitors (or Faradaic SCs).[24] The process of storing energy in the above capacitors is originated in fast reversible redox reactions, which are similar to the processes that happened in batteries. Underpotential deposition, redox pseudocapacitance, and intercalation pseudocapacitance are the basic three different types of redox reactions for pseudocapacitors. The underpotential deposition is a kind of reversible adsorption of metal ions on the different metal surfaces,[25] which is similar to the adsorption between gold and lead ions described in Figure 3A. Redox pseudocapacitance usually happens on the surface of transition metal chalcogenides/nitrides with the Faradaic charge transfer, which is similar to that of RuO_2 shown in Figure 3B. Intercalation pseudocapacitance occurs when ions (e.g., Li^+) intercalate into the tunnels of the redox-active materials, as shown in Figure 3C.[24]

2.3 | Hybrid-capacitors

As shown in Figure 4, hybrid capacitors are the asymmetric SCs (ASCs), which are typically composed of the electrical double-layer (EDL) electrode and the pseudocapacitive or battery-type electrode.[17] These ASCs could provide both high energy density and power density.[26–29] For example, hybrid capacitors based on MXene//Na^+, active carbon//Na^+, carbon//Li^+ exhibited both high energy density and power density.[26–29] Under the operation, the process of the surface adsorption and desorption of the EDLC electrode and the process of the intercalation and deintercalation of the battery-type electrode simultaneously took place, resulting in high energy density at high power density without the degradation in the lifetime.[30] The combination of two different types of electrodes certainly provides a capability to store more energy due to a wide working voltage window created by asymmetric electrodes, and the large specific capacity induced by the battery-type electrode. The rate of charging and discharging still maintains a relatively high level ascribing to the EDLC type electrode. The ASCs possess advanced energy storage for

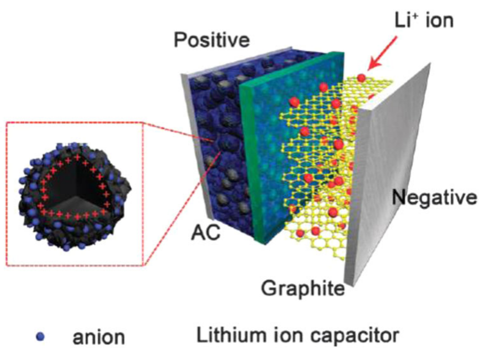

FIGURE 4 Schematic diagram of a hybrid-capacitor. Reproduced with permission: Copyright 2015, Royal Society of Chemistry[17]

commercial applications. However, compared to the EDLC electrodes, the electrochemical performances of ASCs exhibited relatively low-rate energy storage behaviors due to the battery-type electrodes, originating in the sluggish ion/electron diffusion.[31–36] For instance, ASCs reported by Amatucci et al.,[37] utilized the activated carbon (AC) as the positive electrode and $Li_4Ti_5O_{12}$ (LTO) as the negative electrode and reported an energy density of 20 Wh/kg, which was approximatively three times higher than that from the conventional supercapacitor.[37,38] Further studies of ASCs based on the LTO as the negative electrode were also reported.[39,40] In principle, metal oxides, such as MnO_2, RuO_2, and Fe_3O_4 could exhibit their theoretical capacity with relatively low voltage plateau, indicating their potentials as the electrode materials for ASCs to achieve high energy density.

To develop high-performance flexible SCs, the main challenges are to develop high-performance flexible electrodes and solid-state flexible electrolytes.[41] In the following parts, an overview of the development of both flexible electrodes and solid-state electrolytes in the past few years is summarized.

3 | ELECTRODE MATERIALS FOR THE FLEXIBLE SCs

In SCs, charge storage is mainly dependent on the electrode materials. Thus, the development of high-performance flexible electrodes is the key factor to realizing high-performance flexible SCs. In general, the electrode materials used for the fabrication of flexible SCs were categorized into three types: (1) carbon-based materials with high specific surface area,[42,43] (2) conducting polymers (CP),[44,45] and (3) metal chalcogenides/nitrides.[46,47] In addition, other novel materials such as MXenes,[48] metal-organic frameworks (MOFs)/covalent-organic frameworks (COFs),[49,50] transition-metal dichalcogenides (TMDs)[51,52] are also used as the electrodes for flexible SCs.

3.1 | Carbon-based materials

Carbon-based materials are considered as the most promising electrode materials for the industrialization of flexible SCs.[53] Graphene,[54,55] active carbon (AC),[56,57] and carbon nanotubes (CNTs)[58] have been used in flexible SCs due to their low cost, good electrical conductivity, high chemical stability, lightweight, and wide operating temperature range.[59–61] As the electrodes, these carbon-based materials are used to store energy mainly through adsorption and desorption of the charges at the interface between the electrodes and the electrolytes. Therefore, specific surface area, pore size, structure, and electrical conductivity are important factors to evaluate the physical properties of carbon-based materials. Yao et al.[62] investigated the flexible SCs based on 2D hierarchical porous carbon (2D-HPC) nanosheets, which are shown in Figure 5A. The 2D-HPC nanosheets possess a high surface area of 2406 m^2/g, which results in an energy density of 8.4 mWh/cm^3 for the flexible SCs at a power density of 24.9 mW/cm^3, as well as good cyclic stability (96% retention after 10,000 cycles). In addition, the above flexible SCs exhibited good mechanical properties, for example, after 10,000 bending cycles, the flexible SCs still maintained 78% of the initial volumetric capacitance.

CNTs are another candidate used as the flexible electrodes for the development of flexible SCs due to their good electrical conductivity and mechanical properties. Li et al.[68] reported a specific capacitance of 101 F/g at the current density of 0.2 A/g, an energy density of 30.0 Wh/kg with the potential window from 0.001 to 3.0 V from the flexible SCs based on the anchored AC on the 3D framework through the utilization of CNTs and the reduced graphene oxide (rGO) as the electrodes and organic electrolytes. Zheng et al.[63] developed flexible all-solid-state SCs based on the cellulose nanofibril (CNF)/rGO/CNT hybrid aerogel as the flexible electrodes. These flexible SCs exhibited a specific capacitance of 252 F/g at the current density of 0.5 A/g, and an energy density of 28.4 μWh/cm^2 at the power density of 9.5 mW/cm^2. Figure 5B displays the device structure of the above flexible SCs. These flexible SCs present the potential of carbon composite materials as flexible electrode materials.

Graphene is used as the electrodes for the development of high-performance flexible SCs because of their high electrical conductivity and large surface area. Xiong et al.[64] reported an energy density of 8.4 μWh/cm^2 at the power density of 4.9 mW/cm^2, the capacitance retention of 96.7% after 5000 cycles from the flexible SCs based on the blade-casting of graphene hydrogel and rGO as the electrode (Figure 5C).

It was reported that the surface functional groups and heteroatoms could assist the adsorption of counter ions and then improve the hydrophilicity/lipophilicity of the carbon materials, which could result in a great wettability and rapid electrolyte-ions transport within the micropores.[53,63,64,66,68,69] Jiang et al.[65] introduced various functional groups into the carbon nanocages by the nitric treatment (Figure 5D) and observed increased specific capacitance, from 50 to 96 F/g. Recently, we reported the hydrophilic carbon cloth (HCC), which was prepared by chemical oxidation of commercial carbon cloth and further hydrazine gas reduction process (Figure 5E).[66]

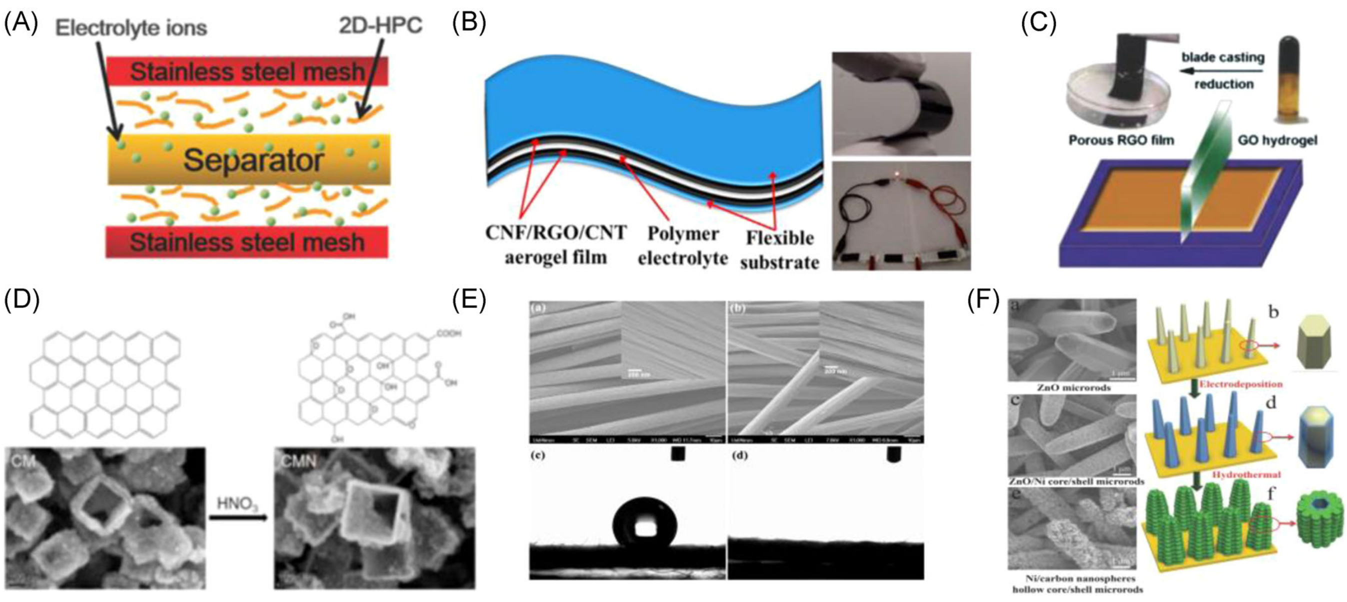

FIGURE 5 (A) Schematic illustration of 2D supercapacitor based on hierarchical porous carbon (2D-HPC). Reproduced with permission: Copyright 2018, John Wiley and Sons.[62] (B) Schematic illustration of supercapacitor with cellulose nanofibril (CNF)/reduced graphene oxide (rGO)/carbon nanotube (CNT) hybrid aerogel electrodes. Reproduced with permission: Copyright 2015, American Chemical Society.[63] (C) Processing of large-area hierarchical graphene films. Reproduced with permission: Copyright 2015, Wiley and Sons.[64] (D) Carbon nanocages with various functional groups. Reproduced with permission: Copyright 2017, Elsevier.[65] (E) Hydrophilic carbon cloth (HCC). Reproduced with permission: Copyright 2019, Wiley and Sons.[66] (F) Schematic illustration of Ni microtube/carbon nanosphere (CNS) composites. Reproduced with permission: Copyright 2015, Wiley and Sons[67]

The HCC fibers exhibited a more rough surface compared to pristine carbon cloths, which indicates that the carbon fibers' surface was modified during the oxidation and reduction processes. In addition, the HCC fibers possessed a completely hydrophilic surface with distinct liquid beads.[66]

Carbon materials combined with pseudocapacitive materials, such as semiconducting polymers and metal oxides, could provide high electrical conductivity and stability.[70–72] Xia et al.[67] developed Ni microtube/carbon nanosphere (CNS) composites as flexible and stable supercapacitor electrodes (Figure 5F). The carbon materials could provide the supporting matrix for metallic microtubes, resulting in enhanced stability of the metallic microtubes. The symmetric SCs with the metal/CNS electrode reach the specific capacitance of 227 F/g at the current density of 2.5 A/g, and the capacitance retention of 97% after 40,000 cycles.

We reported the self-stacked solvated graphene (SSG) films prepared by a facile vacuum filtration method (Figure 6A,B) as the free-standing electrode for flexible solid-state SCs. The highly hydrated SSG films have low mass loading, high flexibility, and high electrical conductivity (Figure 6C,D). The flexible solid-state SCs based on SSG films exhibit excellent capacitive characteristics with a high gravimetric specific capacitance of 245 F/g and good cycling stability of 10,000 cycles (Figure 6E,F). Furthermore, the flexible solid-state SCs

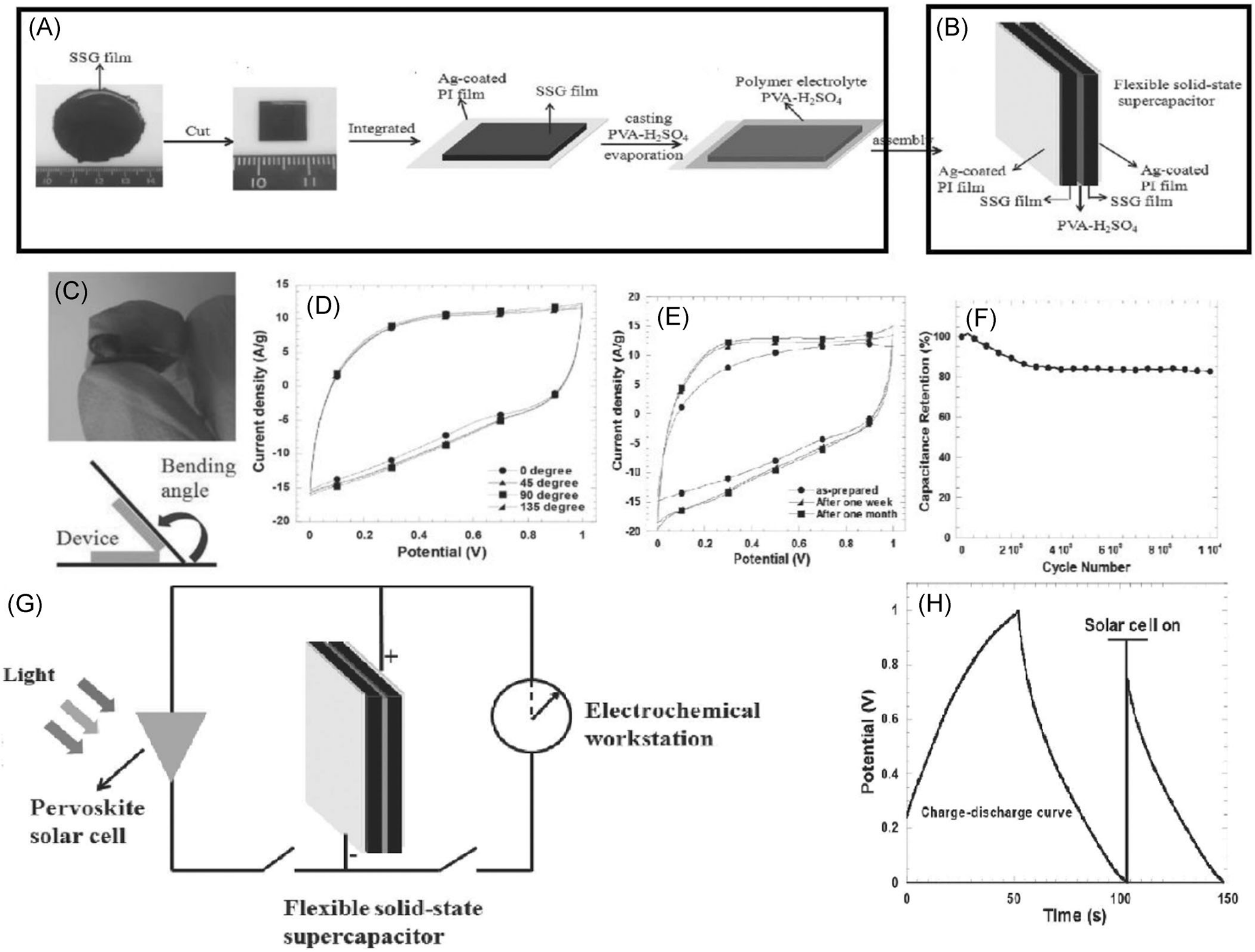

FIGURE 6 (A) Schematically diagram of fabrication of the flexible solid-state supercapacitors (SCs). (B) The device structure of the flexible solid-state SCs. (C) Schematically show how the flexible solid-state SCs were bent and (D) the CV curves of the flexible solid-state SCs scan at 100 mV/s while the devices were bent at different bending angles. (E) The CV curves of the flexible solid-state SCs stored at different time durations with scan rate at 100 mV/s and (F) the cycling stability of the flexible solid-state SCs at the current density of 5 A/g. (G) Schematic diagram of the integration of solid-state SCs with perovskite solar cells and (H) the discharge curve of the flexible solid-state SCs at the current density of 1 A/g after it was charged by perovskite solar cells. CV, cyclic voltammetry. Reproduced with permission: Copyright 2015, Wiley and Sons[73]

were integrated with high-performance perovskite hybrid solar cells to build self-powered electronics (Figure 6G). It was found that the solid-state SCs can be charged by perovskite solar cells and discharged from 0.75 V (Figure 6H). These results demonstrate that the self-powered electronics by integration of the flexible solid-state SCs with perovskite solar cells have great potential applications in the storage of solar energy and flexible electronics, such as portable and wearable personal devices.[73,74] Table 1 summarized the recent works on carbon-based electrodes for SCs.[56,62–64,68,73,75–89]

3.2 | Conducting polymers

Conducting polymers has many advantages as electrodes for the development of flexible SCs. These flexible SCs exhibited wide voltage windows, high storage capacity, and adjustable redox activity.[90–92] Boosted capacitance induced by conducting polymers was through the redox process in which the counterions were transferred to the polymer backbone as the oxidation happened and then was released back to the electrolytes as the reduction process occurred.[93,94] Conducting polymers can be charged with ion insertion in the polymer matrix positively or negatively forming either p- or n-type semiconductors.[53] Polyaniline (PANI),[95,96] polypyrrole (PPy),[97] polythiophene (PTh),[92,98] poly(3,4-ethylenedioxythiophene) (PEDOT),[99,100] and their derivatives are typical conducting polymers used for SCs. However, the swelling and shrinking of conducting polymers occurred during the charging and discharging processes, which results in the mechanical degradation of the electrodes and fading of the electrochemical performance. To address the challenge of low stability, the development of the composites of conducting polymers with other materials is a facile approach.

PANI is one of the most promising materials for CP-based SCs since PANI can be easily synthesized and possesses excellent stability and reversible doping/de-doping process.[101–103] In addition, PANI can be easily polymerized in an aqueous solution to generate polymer thin film with different morphologies. Zang et al.[104] synthesized graphene/PANI fabric composites by electropolymerization. After adding PANI as pseudocapacitive materials, the specific capacitance was increased from 2 to 23 mF/cm^2 without significant degradation after 2000 cycles. Moreover, after 500 times bending, the specific capacitance remained stable (Figure 7A). Chen et al.[105] reported the tandem graphene/PANI SCs by directly growing graphene-PANI electrodes on the separators. The tandem SCs demonstrated the energy density of 26.1 Wh/kg at the power density of 3000 W/kg, and excellent stability after 10,000 cycles (Figure 7B).

Poly(3,4-ethylenedioxythiophene) (PEDOT) is another promising conducting polymers used for the development of SCs. The conjugated backbone of PEDOT allows the delocalized electron transport through the whole system, which leads to a good electrical conductivity.[109–111] Figure 7C reveals the cellulose-mediated PEDOT:Polystyrene sulfonate (PSS)/MWCNT composite film as supercapacitor electrodes.[106] This composite was assembled by incorporating MWCNTs into the cellulose/PEDOT:PSS, exhibiting low resistance of 0.45 Ω with a high specific capacitance of 485 F/g, and good cycling stability with a capacity retention of 95% after 2000 cycles. Anothumakkool et al.[107] developed a highly conducting PEDOT/cellulose paper flexible electrode by interfacial polymerization at the interface of two immiscible liquids (Figure 7D). The all-solid-state SCs fabricated by the PEDOT/cellulose paper flexible electrodes and PVA-H_2SO_4 electrolytes exhibited a specific capacitance of 115 F/g, an energy density of 1 mWh/cm^3, and excellent stability after 3800 charge/discharge cycles.

Besides traditional conducting polymers, some new molecules with the large conjugated system are also synthesized and used as SCs electrodes. Li et al.[108] reported a conjugated polymer gel, poly(4,7-bis(2,3-dihydrothieno[3,4-b][1,4]dioxin-5-yl)benzo[c][1,2,5] thiadiazole (DEBT)-co-tris(4-(2,3-dihydrothieno[3,4-b][1,4] dioxin-5-yl)phenyl) amine (TETPA), for approaching high-performance electrodes. The structure of P(DEBT/TETPA) is shown in Figure 7E. The large conjugated skeleton improved both electrical conductivity and ionic conductivity. The electrodes based on the above materials displayed a good specific capacitance of 149 F/g and a wide voltage window of 1.3 V, as well as the cyclic stability of 92% retention after 2000 cycles. Table 2 summarized the recent works on CP-based electrodes for SCs.[104,106,107,112–117]

3.3 | Metal chalcogenides/nitrides

Metal chalcogenides or nitrides can provide a much higher energy density than conventional carbon-based materials and better electrochemical stability than conducting polymers. They store the energy not only like the electrostatic carbon materials but also show electrochemical redox reactions between electrode materials and electrolyte ions within the potential windows.[33,118–120]

In general, metal chalcogenides/nitrides used as the SCs electrodes are required to meet the following criteria[93]: (1) the chalcogenides/nitrides should be electronically conductive; (2) the metal can exist in two or more oxidation states, which coexist in a continuous

TABLE 1 Summary of recently reported carbon-based electrodes for supercapacitors

Electrode materials	Specific capacitance	Voltage window	Electrolyte	Reference
Activated carbon	88 mF/cm^2 at 10 mV/s	0 to 1 V	1 mol/L H_2SO_4	[56]
2D hierarchical porous carbon nanosheets (2D-HPCs)	250 F/g at 0.5 A/g	0 to 4 V (whole device)	EMIIMBF$_4$ (26 mg/20 µl)/cellulose film	[62]
Activated carbon/carbon nanotube/reduced grapheme oxide (AC/CNT/rGO)	101 F/g at 0.2 A/g	0 to 3 V (whole device)	1 mol/L of $LiClO_4$ in ethylene carbonate (EC) and diethyl carbonate (DEC)	[68]
Single walled carbon nanotube (SWCNT)	34.2 F/g at 0.63 A/g	0 to 2 V (whole device)	PMMA (polymethylmethacrylate)/PC (propylene carbonate)/ACN (acetonitrile)/TBAPF$_6$	[75]
Activated carbon cloth	486 mF/cm^2 at 2 mA/cm^2	0 to 1 V	1 mol/L H_2SO_4	[76]
Activated carbon	110 F/g at 1 A/g	0 to 1 V (whole device)	Potassium hydroxide mesoporous cellulose membrane	[77]
CNT sheet	1.84 mF/cm^2 at 1 µA	0 to 0.8 V (whole device)	PVA/H_3PO_4	[78]
Graphene sheets	11.3 mF/cm^2 at 1 mV/s	0 to 0.8 V (whole device)	PVA/H_2SO_4	[79]
Multilayer graphene (MG)/multi-walled carbon nanotubes (MWCNTs)	740.9 mF/cm^2 at 1 mA/cm^2	0 to 0.8 V (whole device)	PVA/H_3PO_4	[80]
CNT	17.5 F/g at 2 A/g	0 to 3 V (whole device)	PS-PEO-PS/([EMIM][NTf$_2$], C-TRI)/ACN	[81]
N-doped rGO	3.4 mF/cm^2 at 20 µA/cm^2	0 to 0.8 V (whole device)	PVA/H_3PO_4	[82]
Graphene network (GN)	4.2 mF/cm^2 at 0.1 µA	0 to 0.8 V (whole device)	PVA/H_3PO_4	[83]
Treated carbon cloth	920 mF/cm^2 at 2 mA/cm^2	0 to 1 V (whole device)	PVA/H_2SO_4	[84]
3D-graphene/graphite	80 F/g at 5 mV/s	0 to 1 V (whole device)	PVA/H_2SO_4	[85]
MWCNTs	2.02 F/cm^3 at 10 mV/s	0 to 0.8 V (whole device)	PVA/H_3PO_4	[86]
MWCNTs	26.8 F/g at 1 A/g	0 to 1 V (whole device)	PVA/H_3PO_4	[87]
Expanded graphite foil	30.5 mF/cm^2 at 1 mA/cm^2	0 to 1 V (whole device)	PVA/H_2SO_4	[88]
Self-supporting flexible and transparent graphene film (STF-GF)	4.21 mF/cm^2 at 0.1 mA/cm^2	0 to 1 V (whole device)	PVA/H_2SO_4	[89]
Cellulose nanofibril (CNF)/reduced graphene oxide (rGO)/carbon nanotube (CNT)	252 F/g at 0.5 A/g	0 to 1 V (whole device)	PVA/H_2SO_4	[63]
rGO	71.0 mF/cm^2 at 1 mA/cm^2	0 to 1 V (whole device)	1 mol/L H_2SO_4	[64]
Self-stacked solvated graphene (SSG)	245 F/g at 1 A/g	0 to 1 V (whole device)	PVA/H_2SO_4	[73]

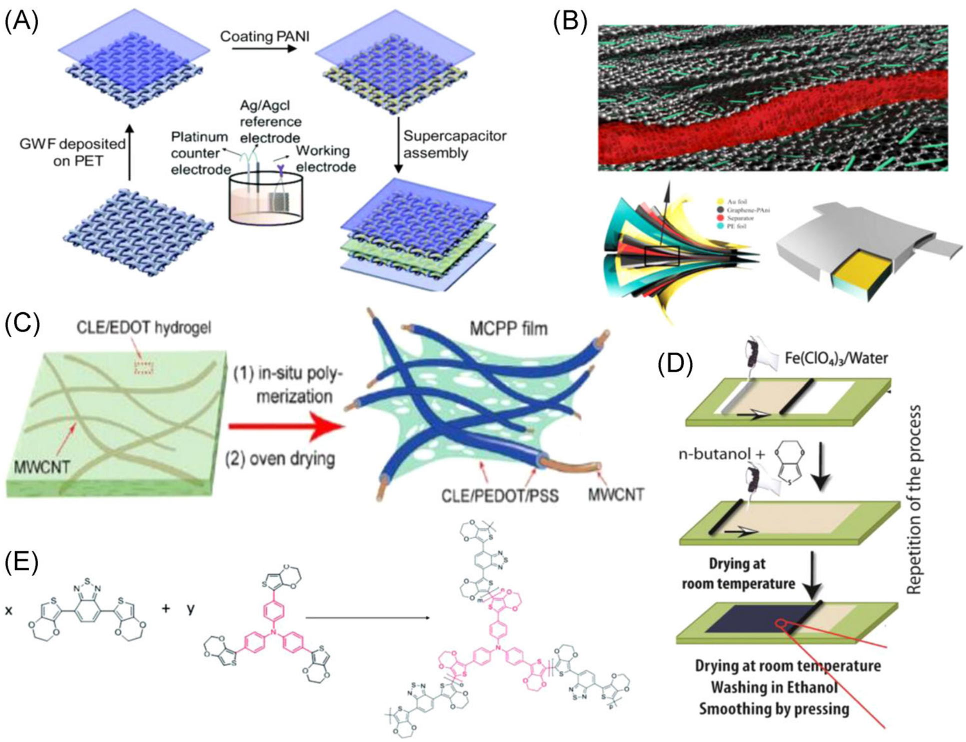

FIGURE 7 (A) Schematic illustration of graphene/polyaniline (PANI) fabric composites. Reproduced with permission: Copyright 2015, Royal Society of Chemistry.[104] (B) Schematic illustration of the tandem graphene/PANI supercapacitors. Reproduced with permission: Copyright 2015, Elsevier.[105] (C) Schematic illustration of the cellulose-mediated poly(3,4-ethylenedioxythiophene: Polystyrene sulfonate/multiwall carbon nanotubes composite films. Reproduced with permission: Copyright 2017, American Chemical Society.[106] (D) Schematic illustration of the processing of conducting poly(3,4-ethylenedioxythiophene)/cellulose paper flexible electrodes. Reproduced with permission: Copyright 2015, Royal Society of Chemistry.[107] (E) The structure of P{poly(4,7-bis(2,3-dihydrothieno[3,4-b][1,4]dioxin-5-yl) benzo[c][1,2,5] thiadiazole(DEBT)-co-tris(4-(2,3-dihydrothieno[3,4-b][1,4]dioxin-5-yl)phenyl) amine (TETPA)}. Reproduced with permission: Copyright 2019, Royal Society of Chemistry[108]

range with no phase changes; (3) the protons can freely disperse into the chalcogenides/nitrides lattice on reduction. Based on these requirements, the chalcogenides/nitrides of ruthenium, manganese, cobalt, nickel, and vanadium are commonly used as the electrode materials of SCs.

Ruthenium oxides (RuO_2) are considered the most extensively studied candidates since they can provide a wide potential window, highly reversible redox reactions, high proton conductivity, and high specific capacitance.[121–123] Wang et al.[122] introduced ripple-like ruthenium oxide (RuO_2)/CNT composites synthesized by using cathodic deposition technique, as shown in Figure 8A. The composites exhibited a specific capacitance of 272 mF/cm^2. Moreover, the symmetric cells, using the composites as the electrodes, possessed a high specific capacitance of 37.23 mF/cm^2 and a specific power density of 19.04 mW/cm^2. Although RuO_2 can provide an extremely high specific capacitance, the high cost and environmental harmfulness prevent it from the commercialization of SCs.[131]

Manganese oxides (MnO_2) as an alternative material has been rapidly developed since they have advanced features such as low cost, environmentally friendliness, low toxicity, and great theoretical capacitances (ranging from 1100 to 1300 F/g) which is depended on the redox reaction as described by the following equation[132–134]:

$$MnO_2 + C^+ + e^- \leftrightarrow MnOOC, \quad (2)$$

where C^+ denotes the protons and alkali metal cations in the electrolyte; e^- stands for the electrons. Moreover, among the transition metal oxides, MnO_2 has the easiest and low-cost approach to synthesize, for example, by the traditional hydrothermal method[135–137] and electrochemical deposition.[138–140] Figure 8B shows the fibrous PANI@MnO_2 nanocomposite, which was reported by Ansari et al.[124] This material exhibited a high capacitance of 525 F/g and excellent cycling stability of 76.9% after 1000 cycles. Lv et al.[126] directly formed the flexible electrodes with the ultralong MnO_2 nanowire composites. The hive-like stretchable SCs exhibited a specific

TABLE 2 Summary of recently reported conducting polymers-based electrodes for supercapacitors

Electrode materials	Specific capacitance	Voltage window	Electrolyte	Reference
Multiwall carbon nanotubes-reinforced cellulose/PEDOT:PSS film (MCPP)	380 F/g at 0.25 A/g	0 to 1 V (whole device)	Polyvinyl alcohol (PVA)/potassium hydroxide	[106]
rGO/polypyrrole (PPy)	147.9 F/cm^3 at 5 A/cm^3	0 to 0.8 V (whole device)	PVA/H_2SO_4	[112]
PPy	702 mF/cm^2 at 1 mA/cm^2	0 to 0.8 V (whole device)	PVA/H_3PO_4	[113]
Polyaniline (PANI)	237.5 mF/cm^2 at 10 mV/s	−0.6 to 0.6 V	PVA/H_2SO_4	[114]
rGO/PANI	6.4 mF/cm^2 at 0.08 mA/cm^2	0 to 1 V (whole device)	PVA/H_2SO_4	[115]
poly(3,4-ethylenedioxythiophene (PEDOT):PSS	202 F/cm^3 at 0.54 A/cm^3	0 to 0.8 V (whole device)	PVA/H_2SO_4	[116]
rGO/PPy	0.51 F/cm^2 at 0.1 mA/cm^2	0 to 0.8 V (whole device)	PVA/H_3PO_4	[117]
Graphene woven fabric (GWF) and PANI	23 mF/cm^2 at 0.1 mA/cm^2	−0.5 to 0.5 V (whole device)	PVA/H_3PO_4	[104]
PEDOT/cellulose paper	115 F/g	0 to 1.2 V (whole device)	PVA/H_2SO_4	[107]

Abbreviation: PSS, polystyrene sulfonate.

capacitance of 227.2 mF/cm^2, 500% elongation without electrochemical performance decay, and 98% capacitance retention after 10,000 stretch-and-release cycles under 400% tensile strain (Figure 8D).

Nickel oxides are considered as promising alternative electrode materials for SCs due to their ultrahigh theoretical specific capacitance, nontoxicity, and low cost.[141–143] The redox reaction of nickel oxides is expressed as the following equation:

$$NiO + OH^- \leftrightarrow NiOOH^- + e^-. \quad (3)$$

The theoretical specific capacitance is calculated to be 3750 F/g, which is much higher than that of manganese oxides.[144] Wang et al.[125] developed FeOF/Ni$(OH)_2$ core-shell composites as the flexible positive electrodes. FeOF has a low intrinsic resistance, which can enhance the charge transfer process. Large-surface Ni$(OH)_2$ could provide enough capacitance for the asymmetric SCs (Figure 8C). The composite electrodes exhibited a high specific capacitance of 1425 F/g at a current density of 1 A/g. Guan et al.[127] reported a porous $NiCo_2O_4$ nanostructure as the flexible electrode for SCs. The full cells exhibited an energy density of 31.9 Wh/kg at a power density of 2.9 kW/kg, and 86.7% capacitance retention after 20,000 cycles (Figure 8E).

Vanadium oxides are also promising candidates for the Faradic electrode materials due to their variety of oxidation states of vanadium ions, low cost, and low toxicity.[145–147] However poor electrical conductivity was a bottleneck, restricting further development of the vanadium-based electrodes.[148,149] To enhance the electrical conductivity of the vanadium-based electrodes, lots of vanadium-based composites have been developed.[149,150] Foo et al.[128] developed the flexible V_2O_5-rGO composite electrode. Due to the high electrical conductivity of rGO, the free-standing electrodes have a low sheet resistance without any current collectors. The V_2O_5-rGO composite electrodes exhibited a specific capacitance of 178.5 F/g at a current density of 0.05 A/g, and a wide working potential range of 1.6 V in nonaqueous electrolytes (1 mol/L $LiClO_4$ in propylene carbonate). The rGO/V_2O_5-rGO (VGO) asymmetric SCs presented a low equivalent series resistance of 3.36 Ω with around 20 mg active materials, the maximum energy density of 13.3 Wh/kg, and good flexibility and cyclic stability (the Nyquist plot is shown in Figure 8F). Boukhalfa et al.[151] investigated the high-performance electrodes with MWCNT-vanadium oxide composite materials. By optimizing the film thickness of vanadium oxide coated on the MWCNT, the selected electrodes possessed a remarkable capacitance of up to 1550 F/g.

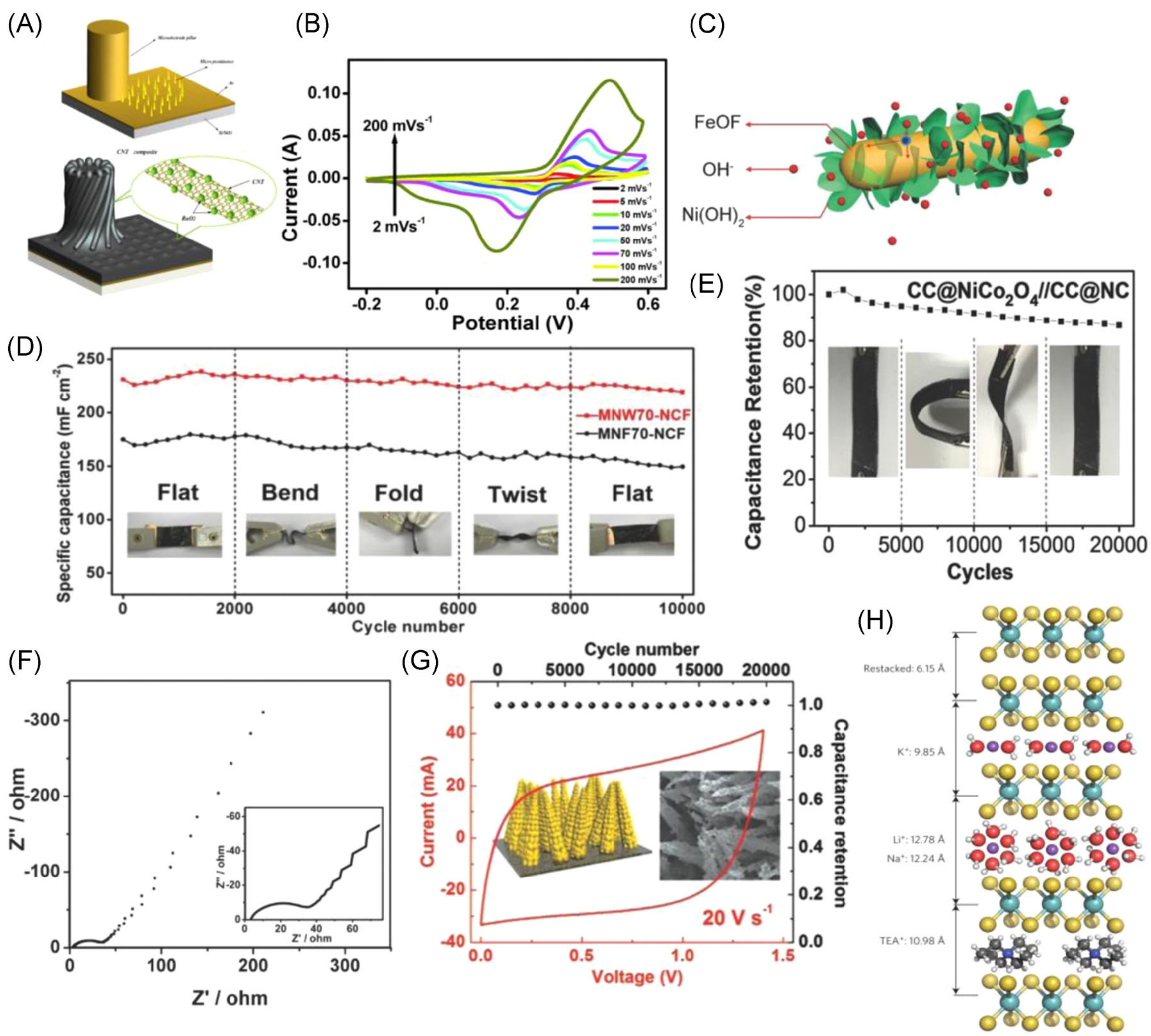

FIGURE 8 (A) Schematic illustration of ripple-like ruthenium oxide (RuO_2)/carbon nanotubes (CNT) composites. Reproduced with permission: Copyright 2015, Elsevier.[122] (B) The cyclic voltammetry curves of fibrous polyaniline (PANI)@MnO_2 nanocomposites. Reproduced with permission: Copyright 2016, Royal Society of Chemistry.[124] (C) Schematic illustration of FeOF/$Ni(OH)_2$ core-shell composites. Reproduced with permission: Copyright 2017, Wiley and Sons.[125] (D) Cyclic stability of the supercapacitors (SCs) based on ultralong MnO_2 nanowire composite electrodes. Reproduced with permission: Copyright 2018, Wiley and Sons.[126] (E) Cyclic stability of the SCs based on porous $NiCo_2O_4$ electrodes. Reproduced with permission: Copyright 2017, Wiley and Sons.[127] (F) The Nyquist plot of SCs based on V_2O_5-rGO composite electrodes. Reproduced with permission: Copyright 2014, Wiley and Sons.[128] (G) SCs with corn-like TiN as the electrodes. Reproduced with permission: Copyright 2016, Creative Commons CC BY license.[129] (H) Schematic illustration of the intercalation behaviors between 1T phase MoS_2 and the ions in the electrolytes. Reproduced with permission: Copyright 2015, Springer Nature[130]

Iron oxides are a common electrode that owns the redox reaction during the charging–discharging processes. Ferroferric oxide is a representable material that can occur value changes of the iron ions. Nevertheless, Fe_3O_4 cannot own excellent structural stability so its structural stability needs to be strengthened by viable and easy methods. Li et al.[152] proposed a solution called "carbon shell-protection" and further reported on a ferroferric oxide-carbon (Fe_3O_4-C) binder-free nanorod array anode, which exhibited dramatically improved cyclic stability after 5000 cycles. This device has a high capacity of 7776.36 C/cm^3 in an alkaline electrolyte, and both high energy and power densities (1.56 mWh/cm^3; 0.48 W/cm^3).

Transition metal nitrides could provide pseudocapacitance by redox reactions, generating high electrical conductivity. For example, the electrical conductivity of titanium nitride (TiN) can reach the range of 4000 to

55,500 S/cm, which is close to those of metals.[153,154] The high electrical conductivity makes the transition metal nitrides become an emerging material for approaching high-performance electrodes.[155–157] Yang et al.[129] developed a corn-like TiN as the electrode for SCs. The symmetric SCs with the TiN electrode exhibited the specific capacitance of 20.7 F/cm^3, the maximum energy density of 1.5 mWh/cm^3, the maximum power density of 150 W/cm^3. In addition, the above SCs exhibited extremely stable performance. After 20,000 charge/discharge cycles, no significant change was observed in the electrochemical performance (Figure 8G).

The 2D transition metal chalcogenides are considered the ideal materials for next-generation electronics due to their ultrathin thickness, high transparency, and excellent electronic properties.[158–163] Recently, Acerce et al.[130] studied the intercalation behaviors between 1T phase MoS_2 and the counterions in the electrolytes (such as H^+, Li^+, Na^+, K^+, and TEA^+) (Figure 8H). 1T MoS_2 exhibited a remarkable capacitive behavior in both aqueous and organic electrolytes. The SCs reached the specific capacitance in the range of 400–700 F/cm^3, the energy density of 0.11 Wh/cm^3 at the power density of 1.1 W/cm^3. In addition, the SCs remained 90% of their initial capacitance after 5000 charge/discharge cycles.

Similar to MoS_2, Shen et al.[160] reported sheet-like $MoSe_2$ grown on the surface of the carbon nanofibers by electrospinning and selenization (Figure 9). The $MoSe_2$/C-700 (selenization at 700 °C) possesses high stability and improved characters of the insertion and extraction with K^+, resulting in boosted stability. The nonaqueous potassium-based ASCs showed the specific capacity of 81 mAh/g at 100 mA/g over 100 cycles. Moreover, nonaqueous ASCs devices by utilizing the $MoSe_2$/C as the anode and the AC as the cathode, and the 0.8 mol/L KPF_6 as the electrolyte was also reported. As indicated in Figure 9A–I, the AC absorbs the PF_6^- counterion, and stores this counterion on the AC's porous structure. At the same time, the K^+ counterion could be absorbed at the interface between $MoSe_2$ and K_xMoSe_2 during the charging process. Illustrated in Figure 9C, the ASCs showed a good electrochemical capacitance and Coulombic efficiency at 100 mA/g over 100 cycles. In addition, the device maintained the specific capacity of 81 mAh/g with capacitance retention of 59.12% after 100 cycles. The whole charging-discharging process of ASCs

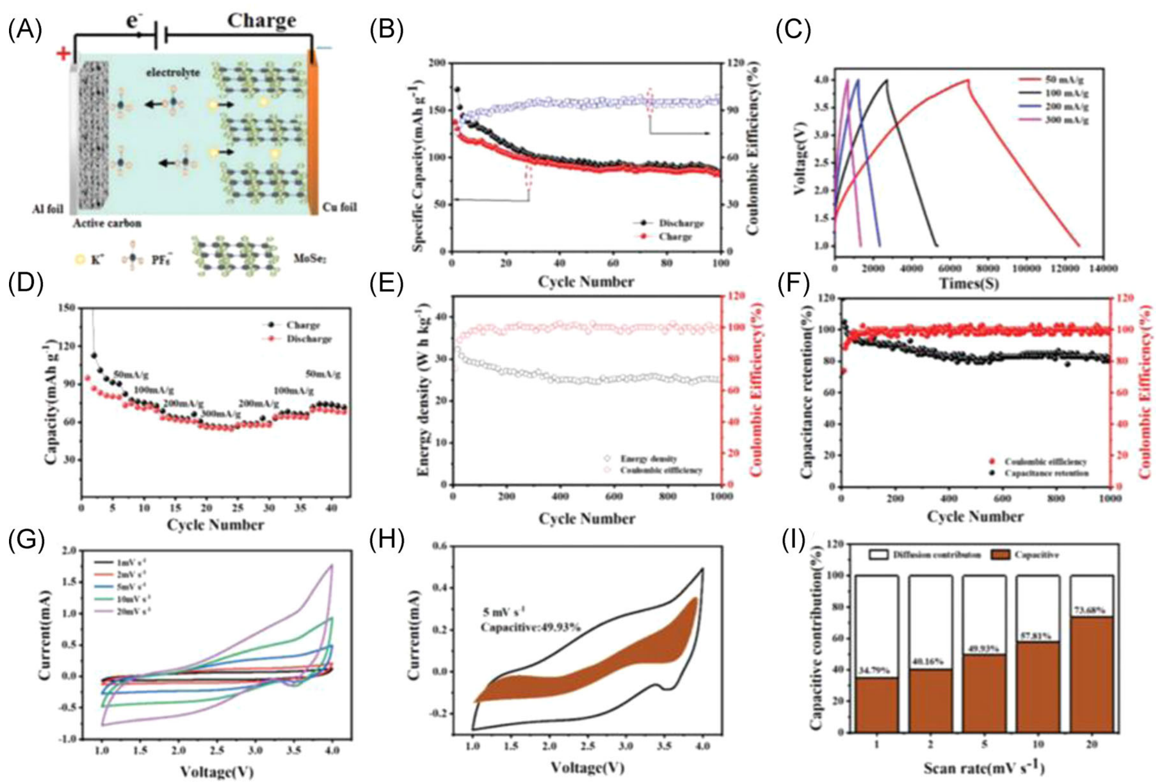

FIGURE 9 (A) The charging process schematic illustration of the asymmetric supercapacitors (ASCs). (B) Cycling performance of ASCs at 100 mA/g. (C) galvanostatic charge-discharge curves at different current densities. (D) Rate performance of ASCs from 50 to 300 mA/g. (E) The cycling stability of the ASCs at 1 A/g. (F) Cycling performance of ASCs at 1.0 A/g. (G) CV curves at different scan rates. (H) The shadow region shows the CV profile with the pseudocapacitive contribution at a scan rate of 5 mV/s. (I) The corresponding percentage of pseudocapacitive contribution. CV, cyclic voltammetry. Reproduced with permission: Copyright 2019, Royal Society of Chemistry[160]

taken 12,000 s at 50 mA/g indicated the ASCs possessed excellent electrochemical performance.

We reported novel $Ni_{0.85}Se@MoSe_2$ nanosheet arrays prepared by a facile one-step hydrothermal method through nickel (Ni) foam as Ni precursor and the framework of $MoSe_2$.[164] The specific performances are displayed in Figure 10. Due to the interconnection and hierarchical porous structure, the $Ni_{0.85}Se@MoSe_2$ nanosheet arrays exhibit a high specific capacitance of 774 F/g at the current density of 1 A/g. Then, we report

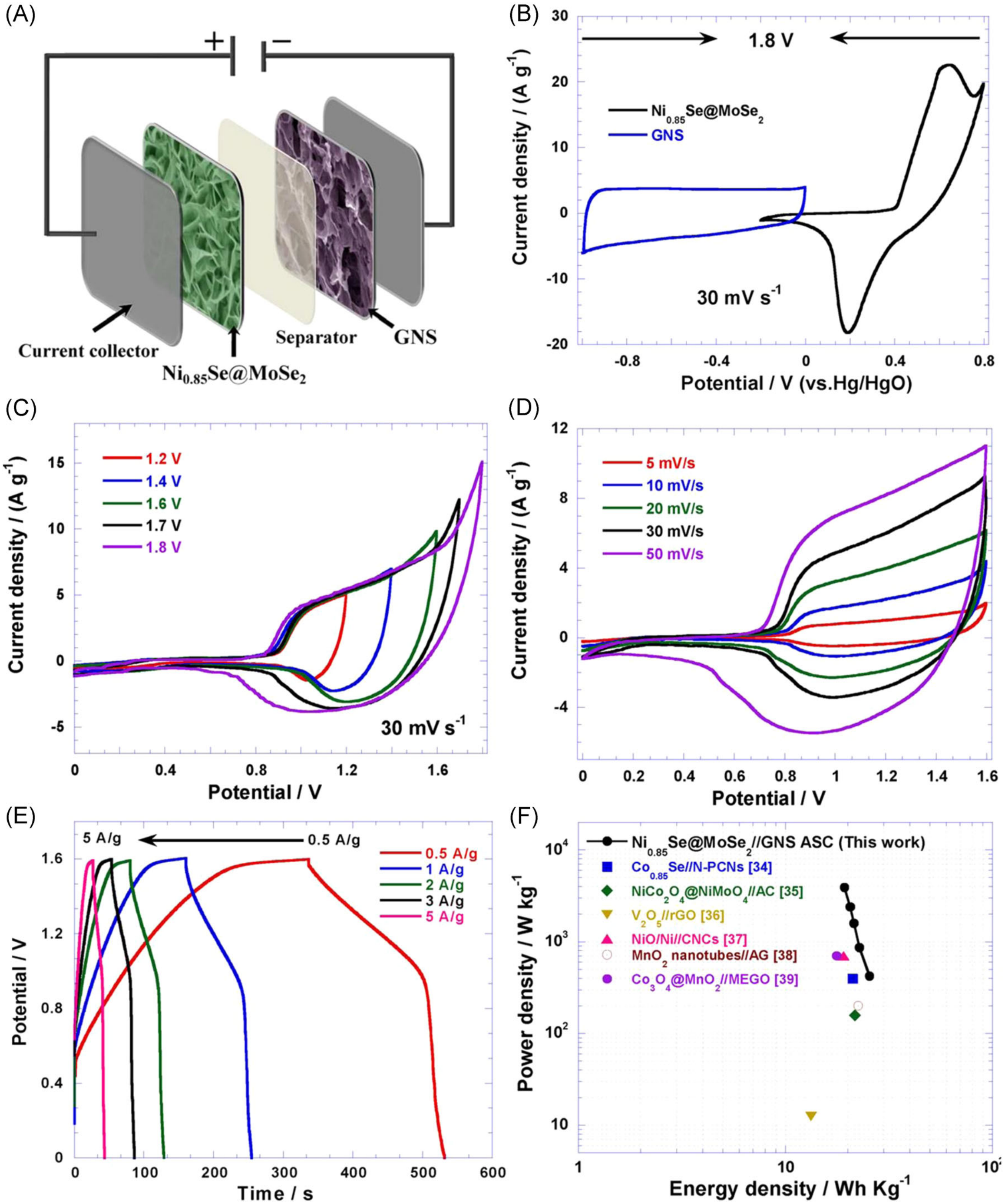

FIGURE 10 (A) Schematic illustration of the $Ni_{0.85}Se@MoSe_2$//graphene nanosheets (GNS) asymmetric supercapacitors (ASCs). (B) Comparative CV curves of the $Ni_{0.85}Se@MoSe_2$ nanosheets and GNS, tested in a three-electrode configuration at 30 mV/s. (C) The CV curves of the $Ni_{0.85}Se@MoSe_2$//GNS ASCs with various potential ranges at 30 mV/s. (D) The CV curves of the $Ni_{0.85}Se@MoSe_2$//GNS ASC at different scan rates. (E) The galvanostatic charge/discharge curves of the $Ni_{0.85}Se@MoSe_2$//GNS ASC at various current densities. (F) The Ragone plots related to energy and power densities of the $Ni_{0.85}Se@MoSe_2$//GNS ASC. CV, cyclic voltammetry. Reproduced with permission: Copyright 2018, American Chemical Society[164]

an ASCs, which is fabricated by using the $Ni_{0.85}Se$@-$MoSe_2$ nanosheet arrays as the positive electrode and the graphene nanosheets (GNS) as the negative electrode, with aqueous potassium hydroxide (KOH) as the electrolyte. The $Ni_{0.85}Se$@$MoSe_2$//GNS ASC possesses an output voltage of 1.6 V, an energy density of 25.5 Wh/kg at a power density of 420 W/kg, and the cycling stability of 88% capacitance retention after 5000 cycles. Table 3 summarized the recent works on metal chalcogenides/nitrides-based electrodes for supercapacitors.[122–129,135,137,140,146,151,155–157,164–168]

3.4 | MXenes

Since discovered in 2011,[169] MXenes, which contain nitrides, transition metal carbides, and carbonitrides, have become an emerging and attracting branch of 2D materials, leading to a rapid expansion of its family.[170] MXenes have a general formula of $M_{n+1}X_nT_x$ ($n = 1 - 3$) where M stands for early transition metal (e.g., Sc, Ti, Zr, Hf, Ta, Cr, and Mo), X is carbon and/or nitrogen while T_x represents the surface terminations (such as oxygen, hydroxyl or fluorine).[169–177] Some of them, for example, $Nb_4C_3T_x$,[171] Ti_2CT_x,[178] and $Ti_3C_2T_x$[179] have been reported. Because of their unique properties, for instance, good mechanical properties, hydrophilicity, and high electrical conductivity (e.g., titanium carbide [$Ti_3C_2T_x$] exhibited a broad electrical conductivity ranging from 1000 to 6500 S/cm[180–183]), MXenes have drawn huge attention as a promising candidate for energy storage applications, including SCs.[177,184]

Compared to the dense stacking feature in the 2D materials, the unique layer-by-layer structure of MXenes could provide a relatively porous structure, which is favorable for ion transport.[156] As it was spontaneously intercalated with metal ions[184,185] and polar organic molecules,[185–187] the electrochemical active cites on the surfaces of MXenes could be occupied by these polar particles, resulting in energy storage subsequently, as indicated in Figure 11A.[188] Hence, increasing the interlayer spacing of MXenes was considered to be an effective way to improve the capacitance of the devices.[48] Yan et al.[48] demonstrated an electrostatic self-assembly method to effectively prevent the self-restacking of MXene nanosheets, through inserting poly(diallyldimethylammoniumchloride) (PDDA)-modified rGO nanosheets between $Ti_3C_2T_x$ layers (Figure 11B). Therefore, the accelerated diffusion of ions in the electrolytes could enable more accessible electroactive sites, resulting in a high volumetric energy density of 32.6 Wh/L for binder-free symmetric SCs. It was also reported that the MXene/rGO electrode exhibited a volumetric capacitance of 1040 F/cm^3 at a scan rate of 2 mV/s, and no significant performance decay after 20,000 charge/discharge cycles. Wen et al.[189] synthesized a new type of nitrogen-doped MXene (N-$Ti_3C_2T_x$) by postetch annealing $Ti_3C_2T_x$ in ammonia. The distance between two layers of MXene sheets increases from 1.92 nm in $Ti_3C_2T_x$ to 2.46 nm in N-$Ti_3C_2T_x$ through treatment at 200 °C with ammonia. As indicated in Figure 11C, THE SCs with the as-synthesized doped MXenes show the capacitances of 192 F/g in 1 mol/L H_2SO_4 and 82 F/g in 1 mol/L $MgSO_4$. Both were higher than those without any treatment. Though hybridization of polypyrrole (PPy) chains with MXene, making PPy chains intercalate into layered Ti_3C_2 (l-Ti_3C_2) (Figure 11D), MXene could effectively prevent the dense PPy stacking, which would benefit the electrolyte infiltration, resulting in high capacitance and good cycling stability.[181] Moreover, the ultra-thin all-solid-state SCs based on the free-stand PPy/l-Ti_3C_2 film exhibited a capacitance of 35 mF/cm^2, stabilized capacitance bent from 0° to 120° (Figure 11E), and nearly 100% capacitance retention over 10,000 charge/discharge cycles was also reported. However, a small voltage window (~0.6 V) was observed from the symmetric SCs based on MXene due to their oxidation at high anodic potentials.[177] To enlarge the voltage window, Jiang et al.[190] reported an all-pseudocapacitive MXene($Ti_3C_2T_x$)-RuO_2 asymmetric SCs (Figure 11F). As a result, an energy density of 37 μWh/cm at a power density of 40 mW/cm (Figure 11G) and 86% capacitance retention after 20,000 charge/discharge cycles (Figure 11H) was achieved from above SCs. Table 4 summarized the recent works on MXene based electrodes for SCs.[48,130,181,189–191]

3.5 | Metal-organic frameworks (MOFs)

MOFs were alternatives for the development of high-performance SCs due to their high porosity and chemical tunability generated by the open channels and nanosized cavities, cursors or sacrificial templates of nanostructured materials.[192–194] MOFs possess advanced features, such as extremely light, well-defined controlled pore sizes, huge pore density, and consequently very high specific surface area (SSA) (e.g., 46,000 m^2/g).[195] Sheberla et al.[49] reported Ni_3(2,3,6,7,10,11-hexaiminotriphenylene)$_2$ ($Ni_3(HITP)_2$), a MOF with high porosity and electrical conductivity (Figure 12A), as the active electrode in EDLCs. Without any conductive additives within MOF, the SCs based on MOF exhibited high gravimetric capacitance of 111 F/g at a scan rate of 50 mA/g and a voltage window of 1V. The SCs also exhibited the capacity retention of more than 90% over 10,000 cycles (Figure 12B). Choi et al.[196] synthesized nanocrystalline MOFs (Figure 12C) incorporated with 2D graphene, and further fabricate the SCs (Figure 12D),

TABLE 3 Summary of recently reported metal chalcogenides/nitrides based electrodes for supercapacitors

Electrode materials	Specific capacitance	Voltage window	Electrolyte	Reference
RuO_2/carbon nanotubes	272 mF/cm^2 at 5 mV/s	−0.3 to 0.7 V	0.1 mol/L Na_2SO_4	[122]
RuO_2/Carbon nanoonions (RuO_2/CNOs)	570 F/g at 1 A/g	0 to 1 V	0.5 mol/L H_2SO_4	[123]
Amorphous MnO_2@multiwall carbon nanotubes (MWCNT) fiber	64 F/cm^3 at 0.2 A/cm^3	0 to 1 V	6 mol/L LiCl	[137]
MnO_2/AC (MAC)	977.4 C/g at 0.2 A/g	−1 to 1 V (whole device)	0.5 mol/L K_2SO_4	[135]
MnO_2	3.04 F/cm^3 at 3 A/cm^3	0 to 0.9 V	1 mol/L Na_2SO_4	[140]
MnHCF-MnO_x	467 F/g at 1 A/g	0 to 0.8 V	0.5 mol/L Na_2SO_4	[165]
FeOF/$Ni(OH)_2$	1452 F/g at 1 A/g	−0.3 to 0.7 V	3 mol/L KOH	[125]
3D V_2O_5	451 F/g at 0.5 A/g	−1 to 1 V (whole device)	1 mol/L Na_2SO_4	[146]
V_2O_5-rGO (VGO)	129.7 F/g at 0.1 A/g	−0.8 to 0.8 V	1 mol/L $LiClO_4$/PC (propylene carbonate)	[128]
TiN@C	124.5 F/g at 5 A/g	−1 to 1 V (whole device)	1 mol/L Na_2SO_4	[155]
Single-crystal GaN mesoporous membrane (GaNMM)	21.1 mF/cm^2 at 10 mA/cm^3	−0.5 to 0.4 V	1 mol/L H_2SO_4	[156]
N-doped carbon coated Nb_4N_5 nanochannels	243.6 mF/cm^2 at 0.5 mA/cm^2	0 to 0.6 V	1 mol/L H_2SO_4	[157]
$Ni_{0.85}Se$@$MoSe_2$	774 F/g at 1 A/g	−0.2 to 0.8 V	2 mol/L KOH	[164]
Polyaniline (PANI)–MnO_2	525 F/g at 2 A/g	−0.2 to 0.6 V	0.5 mol/L H_2SO_4	[124]
MnO_2 nanowire composites	230 mF/cm^2 at 1.6 mA/cm^3	0 to 0.8 V (whole device)	Polyvinyl alcohol/LiCl	[126]
CC@$NiCo_2O_4$	1055 F/g at 2.5 mA/cm^3	0 to 0.6 V	2 mol/L KOH	[127]
MWCNT—vanadium oxide	1550 F/g at 1 A/g	−0.6 to 0.6 V	8 mol/L LiCl	[151]
TiN	20.7 F/cm^3 at 1 V/s	0 to 1.4 V	1 mol/L $LiClO_4$/anhydrous acetonitrile	[129]
Carbon nanotubes/$NiCo_2O_4$	337.3 mF/cm^2 at 0.1 mA/cm^2	0 to 1 V (whole device)	PVA/KOH	[166]
CuO/3D graphene	64 mF/cm^2 at 0.25 mA/cm^2	0 to 0.8 V (whole device)	PVA/LiCl	[167]
Graphene/MoS_2	19.44 F/cm^3 at 0.3 mA	0 to 0.8 V (whole device)	PVA/H_3PO_4	[168]

Abbreviation: KOH, potassium hydroxide.

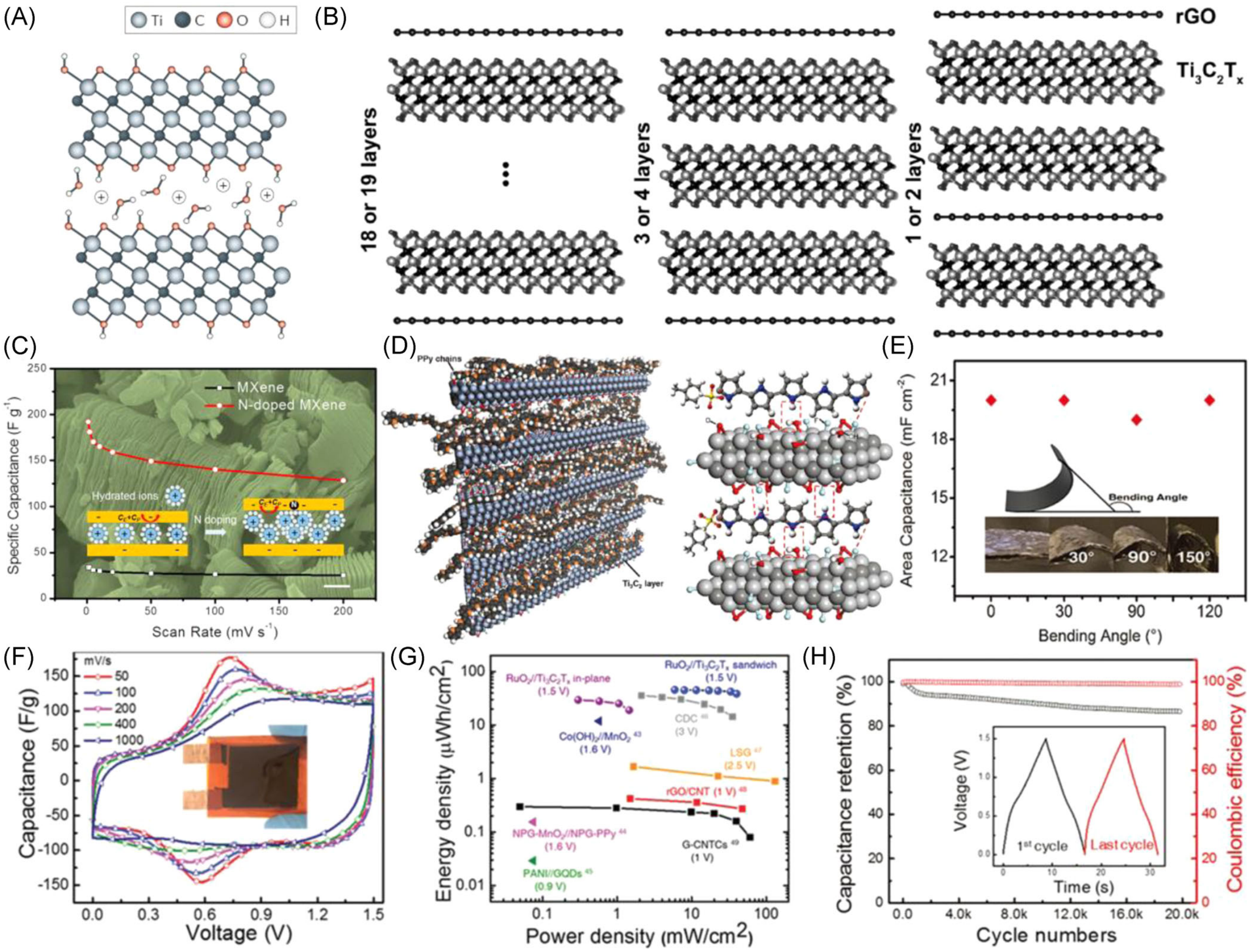

FIGURE 11 (A) Schematic illustration of the intercalation of cation between $Ti_3C_2T_x$ layers. Reproduced with permission: Copyright 2017, Springer Nature.[188] (B) Schematic illustration of MXene/rGO hybrids. Reproduced with permission: Copyright 2017, Wiley and Sons.[48] (C) Schematic illustration of the charge storage process of hydrated electrolyte ions in MXenes (left) and N-doped MXenes (right). Reproduced with permission: Copyright 2017, Elsevier.[189] (D) The left part is a schematic graph of polypyrrole (PPy) intercalated into the l-Ti_3C_2 layers; the right part is the atomic-scale of the schematic illustration. (E) Bending performance of symmetric flexible supercapacitor based on PPy/l-Ti_3C_2 hybrid films. Panels (D,E) reproduced with permission: Copyright 2016, Wiley and Sons.[181] (F) Cyclic voltammetry graphs of the asymmetric sandwich device of RuO_2//$Ti_3C_2T_x$ at different scan rates. (G) Ragone plot of the RuO_2//$Ti_3C_2T_x$ device in comparison to the other microsupercapacitors. (H) Coulombic efficiency and cycling stability of the asymmetric RuO_2//$Ti_3C_2T_x$ device. (F–H) Reproduced with permission: Copyright 2018, Wiley and Sons[190]

TABLE 4 Summary of recently reported MXene based electrodes for supercapacitors

Electrode materials	Specific capacitance	Voltage window	Electrolyte	Reference
PPy/L-Ti_3C_2	203 mF/cm^2 at 1 mA/cm^3	0 to 0.8 V	0.5 mol/L H_2SO_4	[181]
N-$Ti_3C_2T_x$	192 F/g at 1 mV/s	−0.2 to 0.35 V	1 mol/L H_2SO_4	[189]
$Ti_3C_2T_x$/carbon fabric	401 F/g at 10 mV/s	−0.7 to 0.2 V	1 mol/L H_2SO_4	[190]
MXene/rGO-5 wt%	1040 F/cm^3 at 2 mV/s	−0.7 to 0.3 V	3 mol/L H_2SO_4	[48]
$Ti_3C_2T_x$	245 F/g at 2 mV/s	−0.35 to 0.2 V	1 mol/L H_2SO_4	[130]
MXene/graphene	216 F/cm^3 at 0.1 A/cm^2	0 to 0.8 V (whole device)	PVA-H_3PO4	[191]

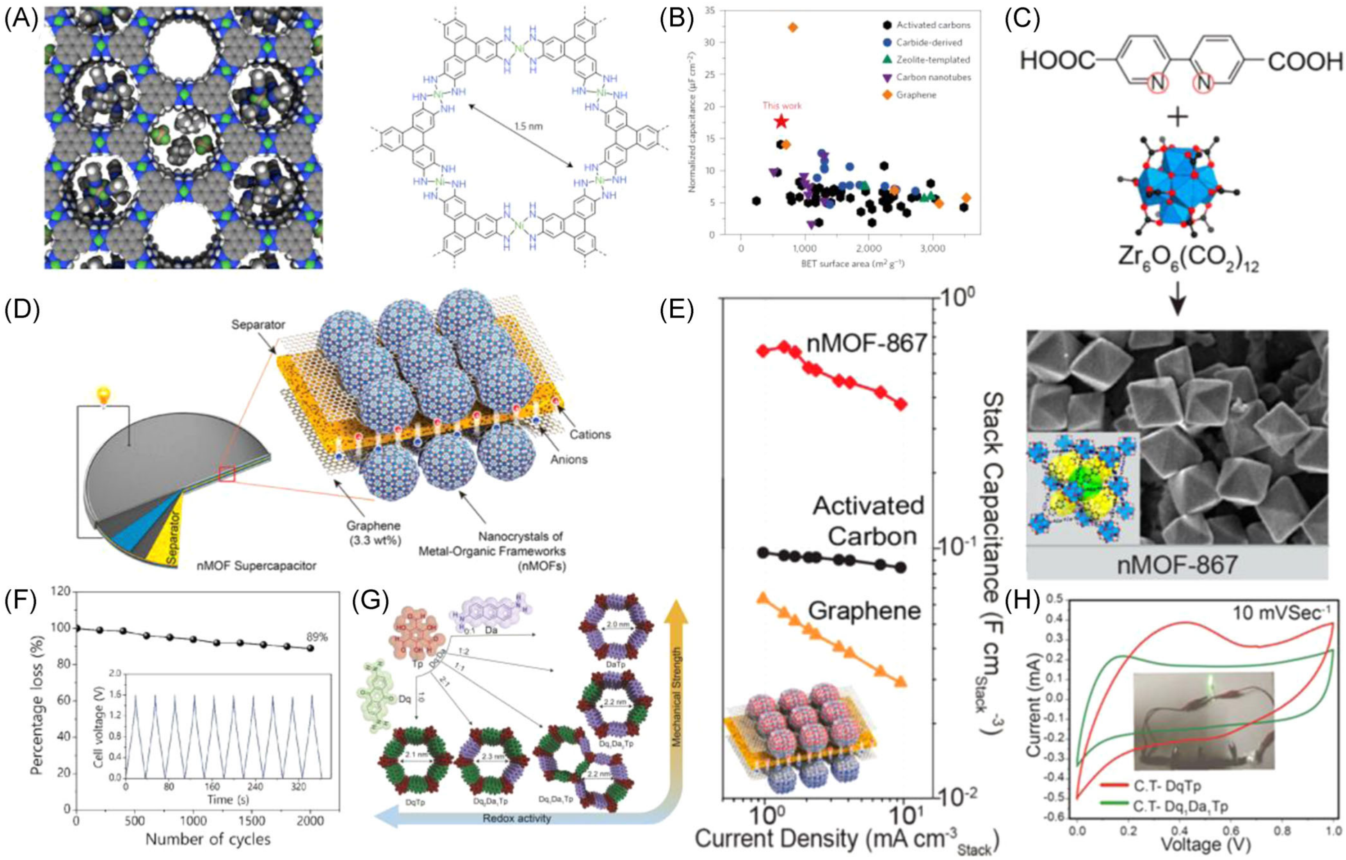

FIGURE 12 (A) The left part is the idealized schematic illustration of relative size of pores in $Ni_3(HITP)_2$ metal-organic frameworks (MOF). White, brown, gray, blue, lime, and green spheres represent H, B, C, N, F, and Ni atoms, respectively. The right part is the molecular structure of $Ni_3(HITP)_2$. (B) Comparison of the areal capacitance of $Ni_3(HITP)_2$ MOF with other EDLC electrode materials. (A,B) Reproduced with permission: Copyright 2017, Springer Nature.[49] (C) Synthetic route, SEM image and idealized schematic illustration of nMOF-867. (D) Idealized schematic illustration of nMOF supercapacitors (SCs). (E) Relationship of stack capacitance of nMOF-867, activated carbon, and graphene versus current density, inset is the schematic image of nMOF SCs. (C–E) Reproduced with permission: Copyright 2014, American Chemical Society.[196] (F) Stability tests of the asymmetric SCs. Reproduced with permission: Copyright 2015, American Chemical Society.[197] (G) Schematic routes of the synthesis of Dq-2,6-diaminoanthraquinone, Da-2,6-diaminoanthracene, and Tp-1,3,5-triformylpholoroglucinol. (H) Cyclic voltammetry curves of CT-DqTp and CT-Dq1Da1Tp covalent-organic frameworks SCs. (G) and (H) Reproduced with permission: Copyright 2018, American Chemical Society[198]

which exhibited a high stack capacitance of 0.64 mF/cm^2, the areal capacitance of 5.09 mF/cm^2 (Figure 12E), and good stability over 10,000 charge/discharge cycles.

However, most synthesized MOFs are nonconductive, which restricted their applications as the electrodes for SCs.[15,194,199,200] But, as porous sacrificial templates and precursors, MOFs have still shown excellent potentials due to their nanostructure and high porosity. Salunkhe et al.[197] developed nanoporous carbon as the negative electrode and nanoporous cobalt oxide (Co_3O_4) as the positive electrode and then sandwiched a single MOF, termed as the zeolitic imidazolate frameworks-67 (ZIFs-67), between two electrodes for making SCs. The as-synthesized nanoporous carbon possessed a high specific surface area (SSA) of 350 m^2/g, and the ZIF-derived nanoporous Co_3O_4 has an SSA of 148 m^2/g. The asymmetric SCs exhibited specific energy of 36 Wh/kg within a voltage window from 0.0 to 1.6 V. This device also represented magnificent rate capability, of which the highest specific power of 8000 W/kg at a specific energy of 15 Wh/kg, within a considerable 2000 cycles stability (Figure 12F).

3.6 | Covalent-organic frameworks (COFs)

Like MOFs, COFs are crystalline materials with high porosity, controllable pore sizes, high surface areas, and highly designed molecular structures.[201–203] However, the building blocks of the COFs are made of light elements, such as H, C, N, and O, and are connected by the covalent bonds. Through various synthetic routes and options, the crystalline structures within COFs can be predictable and well-designed,[198,201] which is comparable to that of MOFs. Since the first successful example of COFs was reported in 2005,[204] this rapidly developed field has increasingly attracted researchers. In 2013, DeBlase et al.[205] described a β-ketoenamine-linked 2D COF, which possessed reversible electrochemical processes of anthraquinone subunit. Moreover, this material exhibited magnificent chemical stability in the strong acidic electrolyte, even to 1 mol/L H_2SO_4. Compared to the non-redox-active one, the modified redox-active COF displayed a higher capacitance (311 F/g) and an energy density (31 Wh/kg) during long-term charge-discharge cycles. Khayum et al.[198] synthesized the convergent COF flexible free-stand thin sheets via the solid-state molecular baking method. As shown in Figure 12G, redox-active 2,6-diaminoanthraquinone (Dq) and π-electron-rich 2,6-diaminoanthracene (Da) are chosen as the linkers in a β-ketoenamine-linked 2D COF. Consequently, the COF thin sheet exhibited redox activity. Moreover, the π-electron-rich anthracene linker could improve the mechanical properties of the free-stand thin sheets through the noncovalent interaction. A symmetrical flexible all-solid-state COF SCs was fabricated by using the peeled carbon tape (CT) as the current collector. The cyclic voltammetry (CV) curves of CT-COF SCs are presented in Figure 12H. The optimized CT-COF SCs exhibited a specific capacitance of 3 F/g and the long-term cyclic stability of 90% capacitance retention after 2500 charge–discharge cycles.

4 | POLYMER-BASED SOLID-STATE ELECTROLYTES FOR FLEXIBLE SCS

As described above, polymer-based solid-state electrolytes act as both electrolytes and separators in SCs. Compared to the conventional liquid electrolytes, the solid-state electrolytes could efficiently prevent the leakage of the toxic liquid electrolytes without the clumsy metal crusts. Moreover, solid-state electrolytes could provide excellent mechanical stability and durability.

Polymer-based solid-state electrolytes are typically composed of three parts: the polymer matrices, the electrolytic salts, and plasticizers. The electrolytic salts and plasticizers are absorbed in the polymer matrices, preventing the leakage of the liquid electrolytes. The polymer matrices include polyvinyl alcohol (PVA),[206–209] polyoxyethylene (PEO),[210–212] polyacrylamide (PAM),[213,214] poly(methylmethacrylate) (PMMA),[215,216] poly(amineester) (PAE),[217,218] and poly(vinylidene fluoride) (PVDF).[219–221] These single and multicomponent polymeric hosts provided good flexibility and stretchability for SCs used in wearable and portable devices. The conducting electrolytic salts and plasticizers also play crucial roles in the solid-state electrolytes. The conducting electrolytic salts and plasticizers can be classified into three types: aqueous electrolytes, organic electrolytes, and ionic liquid electrolytes.

4.1 | Aqueous gel electrolytes

Aqueous gel electrolytes have attracted extensive attention in the past few years due to their high ionic conductivity, low toxicity, ease of processing, and low cost. In the aqueous gel electrolytes, the plasticizer is water. The electrolytic salts in the aqueous gel electrolytes contain strong acids (like H_2SO_4,[222–224] HCl,[225,226] H_3PO_4[104,227,228]), strong bases (KOH[229–231]), or some neutral salts (like Na_2SO_4[232,233] and LiCl[234–236]). Compared to commercial organic electrolytes, these aqueous gel electrolytes are much cheaper and less toxic. Moreover, the high ionic conductivity of the aqueous gel electrolytes leads to low equivalent series resistance (ESR) and high power density. In addition, the aqueous electrolyte could induce a significantly higher specific capacitance compared to the organic systems. The Faradic-active electrode exhibited the highest specific capacitance in the aqueous systems rather than in the organic electrolytes and in the ionic liquids electrolytes, which was ascribed to their high ionic conductivity and small ion radius.[237]

Pan et al.[228] investigated endurable all-solid-state flexible SCs incorporated with MnO_x electrodes and PVA-Na_2SO_4 gel electrolytes (Figure 13A). The flexible SCs exhibited a specific capacitance of 906.6 mF/cm^2 at the current density of 1 A/cm^2, the energy density of 1.16 mWh/cm^3 at the current density of 1 mA/cm^2. No obvious change was observed from the specific capacitance under different binding angles from 0° to 180°. Moreover, the flexible SCs maintained over 85% of their initial capacitance after 200 bending cycles (Figure 13A). Compared to Na^+, Li^+ has a smaller ion radius, leading to higher ionic conductivity.[244,245] Thus, LiCl is another promising electrolytic salt in neutral aqueous systems. Chen et al.[238] recently reported flexible SCs incorporated with the bio-inspired and quasifractal metallic network electrodes and LiCl-PVA gel electrolytes as well (Figure 13B). These flexible SCs also exhibited good long-term mechanical stability. For example, after 500 bending cycles, the flexible SCs kept 93.9% of their initial specific capacitance.

Due to the fast transportation of protons in the aqueous system, the polymer gel electrolytes with

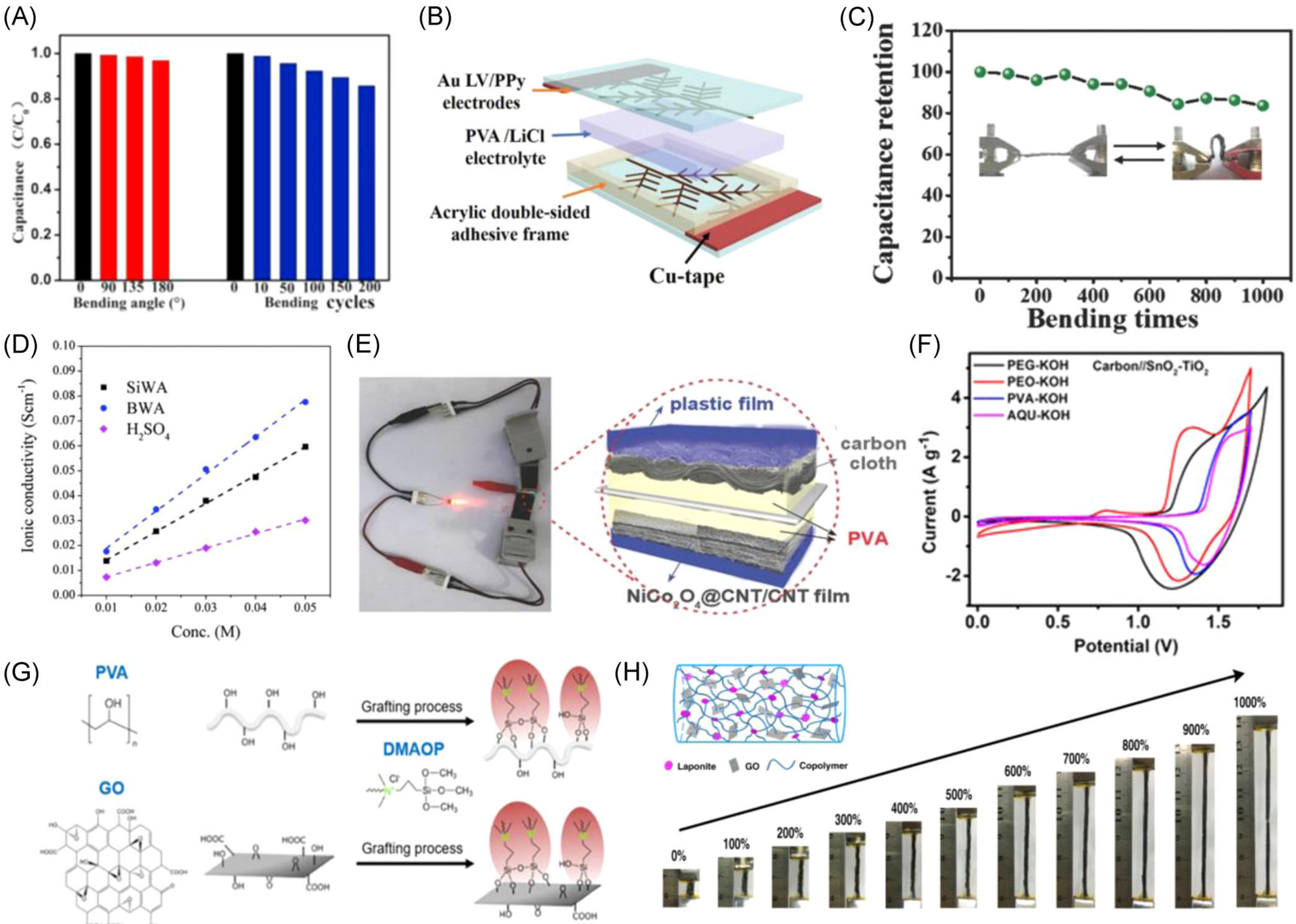

FIGURE 13 (A) Bending stability of supercapacitor with MnO_x electrodes and polyvinyl alcohol (PVA)-Na_2SO_4 gel electrolytes. Reproduced with permission: Copyright 2016, Elsevier.[228] (B) Schematic illustration of supercapacitor with bio-inspired, quasifractal metallic network electrodes and LiCl-PVA gel electrolytes. Reproduced with permission: Copyright 2019, Wiley and Sons.[238] (C) Bending stability of supercapacitor with boron element nanowire electrodes and PVA-H_2SO_4 electrolytes. Reproduced with permission: Copyright 2018, Wiley and Sons.[239] (D) The ionic conductivity of $H_5BW_{12}O_{40}$ (BWA) electrolytes. Reproduced with permission: Copyright 2015, Royal Society of Chemistry.[240] (E) Schematic illustration of supercapacitor with $NiCo_2O_4$@carbon nanotubes electrodes and PVA-KOH gel electrolytes. Reproduced with permission: Copyright 2017, Wiley and Sons.[241] (F) Cyclic voltammetry curves of different polymer matrices in solid-state electrolytes with porous carbon cathode and SnO_2-TiO_2 anode. Reproduced with permission: Copyright 2019, American Chemical Society.[242] (G) Schematic illustration of grafted PVA-KOH gel electrolytes. Reproduced with permission: Copyright 2019, Wiley and Sons.[72] (H) Stretchability of poly(AMPS-co-DMAAm)/laponite/graphene oxide (GO) hydrogel electrolytes. KOH, potassium hydroxide. Reproduced with permission: Copyright 2019, Creative Commons CC BY license[243]

proton-donor acids were widely investigated. These acid gel electrolytes possessed ionic conductivity ranging from 10 to 100 mS/cm at room temperature. Xue et al.[239] reported the sold-state flexible SCs with the boron element nanowire electrodes and the PVA-H_2SO_4 electrolytes. The flexible SCs based on the PVA-H_2SO_4 electrolytes exhibited low internal resistance (1.15 Ω) and charge-transfer resistance (0.64 Ω). In addition, the devices possessed excellent flexibility. After 1000 times bending, the flexible SCs still kept over 80% of their initial capacitance, which was shown in Figure 13C. Gao et al.[240] investigated novel proton-conducting heteropoly acid gel electrolytes for SCs. The $H_5BW_{12}O_{40}$ (BWA) electrolytes possessed a high ionic conductivity than that of H_2SO_4 at the same concentrations (Figure 13D). The SCs exhibited a maximum cell voltage of 1.6 V.

Among different alkaline electrolytic salts in the gel electrolytes, KOH is the most widely used in alkaline gels because of its low cost, high ionic conductivity, and environmental friendliness.[17,53] Wu et al.[241] reported an all-solid-state asymmetric SCs with the $NiCo_2O_4$@CNT electrodes and the PVA-KOH gel electrolytes, which were shown in Figure 13E. The SCs exhibited an energy density of ~27.6 Wh/kg at the power density of 0.55 kW/kg, kept

95% capacitance retention after 5000 cycles. In addition, the SCs maintained their electrochemical performance under different bending angles from 0 to 180°. To investigate the influence of the polymer matrices on the electrochemical performance, Pal et al.[242] evaluated different polymer matrices in the solid-state electrolytes within the porous carbon cathode and the SnO_2-TiO_2 anode. Figure 13F presents the CV curves of different polymer matrices in solid-state electrolytes with porous carbon cathode and SnO_2-TiO_2 anode, the grafted PVA-KOH gel electrolytes, and the stretchability of poly(AMPS-co-DMAAm)/laponite/graphene oxide (GO) hydrogel electrolytes. Among the solid-state electrolytes based on PVA, PEO, and PEG-KOH, the asymmetric SCs based on the PEG-KOH electrolytes exhibited the highest specific capacitance due to their lower bulk and charge transfer resistance, quicker ion diffusion rate, and less ion pairing.

Besides the single-component polymer-based electrolytes, more and more multicomponent polymer gel-based solid-state electrolytes have been developed to further enhance both the electrochemical and mechanical performance. Chen et al.[72] developed a multicomponent PVA-KOH gel electrolyte by grafting graphene oxide and amino groups on the PVA backbone, as shown in Figure 13G. The grafted PVA-KOH gel electrolytes show a much higher ionic conductivity of 108.7 mS/cm than that (30.5 mS/cm) in the pure PVA-KOH gel electrolytes. While enhancing the electrochemical performance, multicomponent polymer gel-based solid-state electrolytes also have impressive improvements in mechanical performance. Recently, Li et al.[243] have investigated a multifunctional hydrogel polyelectrolyte with copolymerization of 2-acrylamido-2-methylpropane sulfonic acid (AMPS) and *N,N*-dimethylacrylamide (DMAAm). The SCs based on poly(AMPS-co-DMAAm)/laponite/GO hydrogel electrolytes show superior mechanical stretchability (up to 1000%) and excellent self-healing behavior under either heating or light treatment (Figure 13H).

4.2 | Organic gel electrolytes

Even though the SCs incorporated with the aqueous electrolytes exhibited decent device performance, the voltage window was small. To enlarge the voltage window, the organic electrolytes have become promising candidates for flexible SCs with a high energy density. The organic gel electrolytes typically were composed of high molecular weight polymer matrices and organic conducting salts, which were dissolved in the aprotic solvents. Nguyen et al.[246] synthesized a solid polymer electrolyte with four interbonding layers. As shown in Figure 14A, linear poly(ethylene imine) (L-PEI) and PEO were used to enhance the solubility of lithium salt and ionic transport. Poly(acrylic acid) (PAA) was served as the bridge to link the L-PEI and PEO. The solid electrolytes exhibited an ionic conductivity of 10^{-5} S/cm at room temperature, which was described by the Vogel–Fulcher–Tammann equation.

In the organic electrolytes, it was found that the organic ammonium salts, such as tetraethylammonium tetrafluoroborate (TEABF4),[251–253] tetrabutylammonium hexafluorophosphate (TBAPF6),[254,255] and bis(trifluoromethylsulfonyl) ($TFSI^-$) amine[256] played the most common roles as the conducting salts. To further increase the device performance, Park et al.[247] added decamethylferrocenium (DmFc) into tetrabutylammonium perchlorate (TBAP)-tetrahydrofuran (THF) electrolytes. The redox reaction of DmFc could provide an extra pseudocapacitance for the flexible SCs. As presented in Figure 14B, after the addition of DmFc redox couples, the voltage widows of the flexible SCs with a device structure of CNT/DmFc-TBAP-THF/CNT were increased from 1.1 to 2.1 V, the energy densities from 1.3 to 36.8 Wh/kg, and the specific capacitances from 8.3 to 61.3 F/g, as compared with those of the SCs without DmFc. It was also found that 1 mol/L TEABF4 dissolved into acetonitrile (AN) and propylene carbonate (PC) exhibited an ionic conductivity of 60 mS/cm, which was over five times larger than that only in PC solution (11 mS/cm).[257] Kötz et al.[248] studied the gas evolution behavior of AN, PC, and γ-butyrolactone (GBL) as solvents in the electrolytes (Figure 14C). The GBL exhibited a significant gas evolution at 2.5 V while PC starts to release gas at 3.0 V and AN keeps low gas evolution rate even at 3.25 V. These results suggested that the electrolytes in AN solution could produce a high-potential window SCs. Moreover, the electrolytes based on PC were more environmental-friendly and safe, which are ascribed to less flammability and toxicity of AN.[47] Recently, mixed solvents have been used to further enlarge the voltage windows. Ramasamy et al.[249] reported a PC: ethylene carbonate (EC): dimethyl carbonate (DMC): sodium bis(trifluoromethanesulfonyl)imide (NaTFSI) mixed system and found out that their ionic conductivity was higher than that from solely solvent. In Figure 14D, the NaTFSI:PC, PEO: NaTFSI:PC, and PEO: PC:EC:DMC:-NaTFSI were corresponding to the systems 1, 2, and 3, respectively. The multisolvent gel electrolytes showed better impedance performance than the single-solvent gel electrolytes. The utilization of the organic gel electrolytes could also broaden the working temperatures due to their low freezing point. Cai et al.[250] investigated a modified polyvinylidene fluoride (PVDF): lithium trifluoromethanesulfonate (LiTFS) polymer electrolytes for the low-temperature solid-state SCs. As shown in

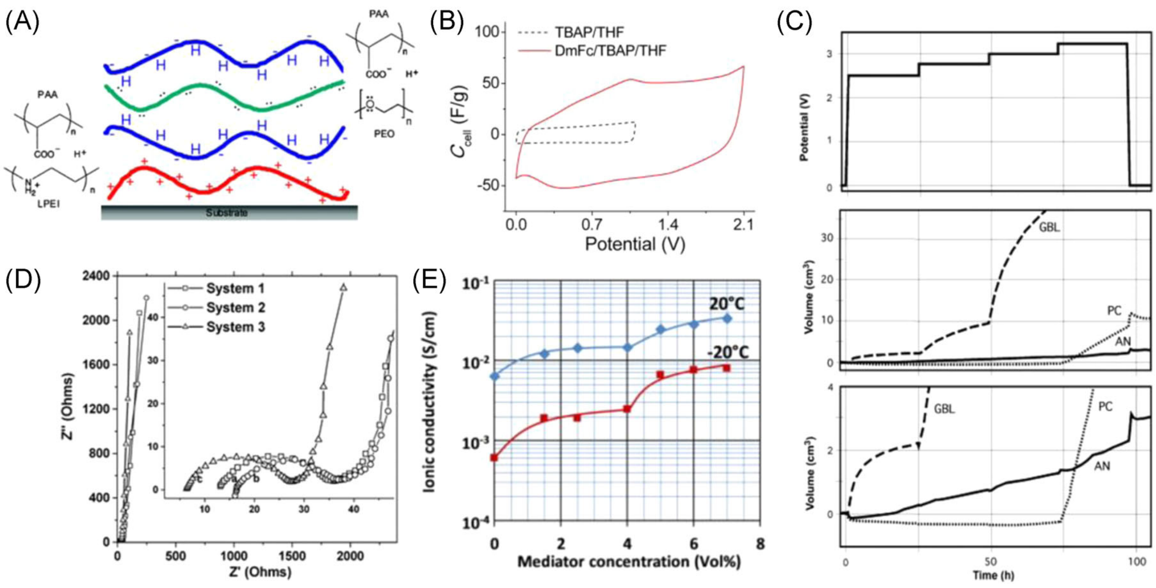

FIGURE 14 (A) Schematic illustration of the polymer electrolyte with four interbonding layers. Reproduced with permission: Copyright 2011, American Chemical Society.[246] (B) Cyclic voltammetry curves of carbon nanotubes (CNT)/DmFc-tetrabutylammoniumhexafluorophosphate-tetrahydrofuran/CNT devices. Reproduced with permission: Copyright 2014, American Chemical Society.[247] (C) The gas evolution behavior of acetonitrile, propylene carbonate (PC), and γ-butyrolactone as the solvents in the electrolytes. Reproduced with permission: Copyright 2008, Elsevier.[248] (D) Nyquist plots of NaTFSI:PC, polyoxyethylene (PEO):NaTFSI:PC, and PEO:PC:ethylene carbonate (EC):dimethyl carbonate:NaTFSI as electrolytes. Reproduced with permission: Copyright 2014, American Chemical Society.[249] (E) Ionic conductivities of the modified poly(vinylidene fluoride)/ithium trifluoromethanesulfonate polymer electrolytes. Reproduced with permission: Copyright 2019, Elsevier[250]

Figure 14E, the modified PVDF/LiTFS polymer electrolytes exhibited an ionic conductivity of ~10^{-3} S/cm at −20 °C and of 10^{-2} S/cm at 20 °C, which indicated that the SCs have great potential applications in various environments. By using nonaqueous solvents, the voltage windows of the organic electrolytes can reach 2.5–3 V,[130,251–253,258] which were dramatically higher than that observed from the aqueous systems. Although the organic electrolytes can provide much larger voltage windows than the aqueous systems, the challenge was that the organic electrolytes are toxic, volatile, flammable, and moisture sensitive. Thus, the SCs with organic electrolytes have to be sealed in the shells to prevent the volatilization of solvents, which restricts their applications in portable or wearable devices.

4.3 | Ionic liquid (IL) gel electrolytes

The solvent-free ILs are regarded as another promising candidate as the solid state-electrolytes for approaching high-performance SCs since large potential windows (up to 6.0 V) can be obtained from these systems.[259] The ILs are a kind of organic salts that are composed of large cations and delocalized anions with low melting points, low vapor pressure, and noninflammability.[260,261] The electrochemical performances of the ILs based electrolytes mainly relied on the chemical structures of counterions used. To select the suitable IL molecules for the SCs, three major parameters, ionic conductivity, working voltage window, and the melting point, should be considered. Several cationic ILs, such as quaternary ammonium,[251,262] sulfonium,[263–265] imidazolium,[266–268] pyrrolidinium,[269,270] piperidinium,[271,272] have been developed. For anionic ILs, tetrafluoroborate (BF_4^-),[251,273,274] hexafluorophosphate (PF_6^-),[275] bis(trifluoromethanesulfonyl)imide ($TFSI^-$),[263,267,272,276,277] bis(fluorosulfonyl)imide (FSI^-),[278,279] dicyanamide (DCA^-)[279,280] were the most common ones. Figure 15 presents the molecular structures of typical ILs. Compared to the organic electrolytes, the ILs based electrolytes could extend the voltage windows of SCs to 3.5–6 V, commonly around 4 V, and remain the high ionic conductivity in the order of 10^{-3} to 10^{-2} S/cm.[20,257,281]

Yang et al.[282] developed a GO doped poly(vinylidene fluoride-hexafluoro propylene (P(VDF-HFP))-1-ethyl-3-methylimidazolium tetrafluoroborate (EMIMBF4) ion gel electrolytes with an ionic conductivity of 25 mS/cm at room temperature. The CV curves of supercapacitor with graphene doped carbon materials and GO-EMIMBF4-(P(VDF-HFP) ion gel are displayed in Figure 16A. The all-solid-state SCs with graphene doped carbon materials and GO-EMIMBF4-(P(VDF-HFP) ion gel as electrodes and electrolytes,

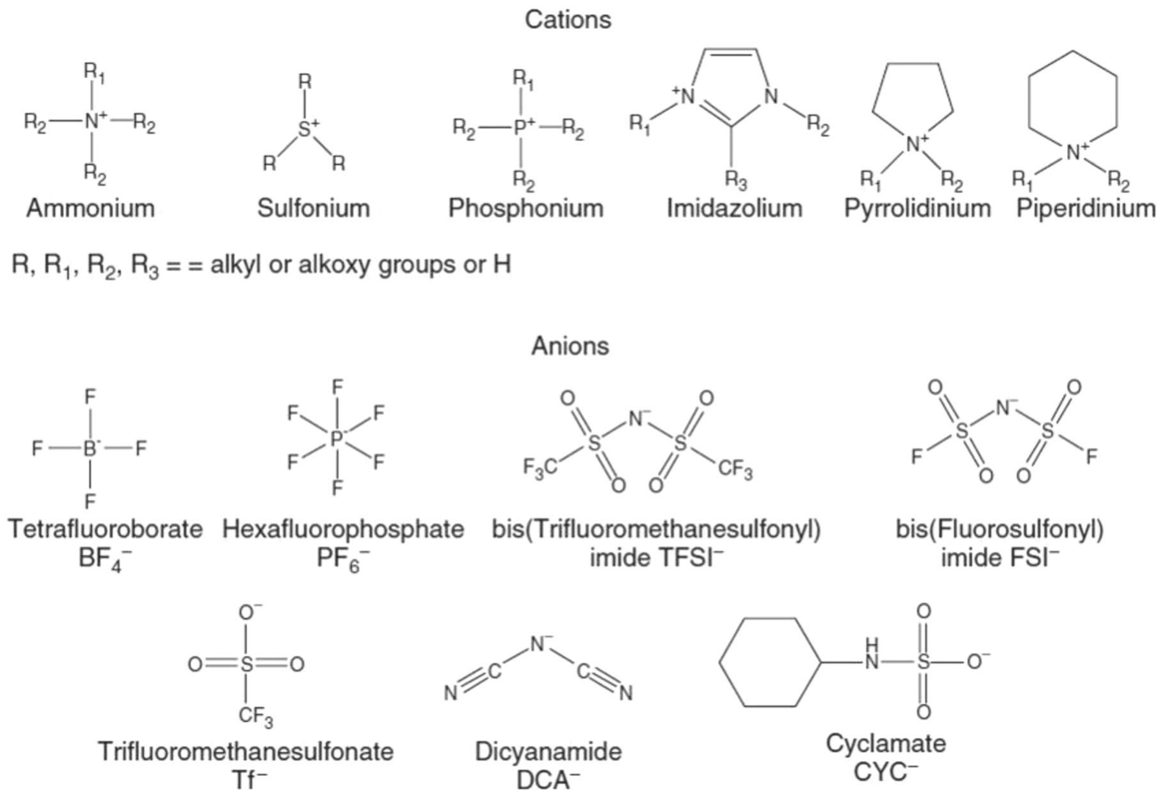

FIGURE 15 The structures of typical ionic liquids ions. Reproduced with permission: Copyright 2013, Wiley and Sons[257]

respectively, exhibited a stable working potential window from 0 to 3.5 V, the specific capacitance of 190 F/g, the energy density of 76 Wh/kg at the current density of 1 A/g. She et al.[283] investigated high-voltage SCs with ILs decorated GO and polypropylene (PP):EMIMTFSI as the electrodes and the electrolyte, respectively. The surfactant microemulsion system of ILs can accelerate the diffusion of ionic liquid ions into GO. The SCs based on the above electrode and electrolytes exhibited a working window of 3 V, the specific capacitance of 302 F/g, the maximum energy density of 45 Wh/L at the power density of 571.4 W/L at RT. The Ragone plot is displayed in Figure 16B. In addition, the SCs based on ILs electrolytes exhibited excellent stability in a wide temperature ranging from −95 °C to more than 300 °C,[257,286] which was inaccessible in the aqueous electrolytes and the organic electrolytes. Pandey and Hashmi[284] reported a 1-ethyl-3-methylimidazolium tetracyanoborate (EMIMTCB) entrapped in poly(vinylidene fluoride-co-hexafluoropropylene) (PVdF-HFP) gel electrolytes, which could provide a wide working window of about 3.8 V and high ionic conductivity of 9×10^{-3} S/cm at RT (as shown in Figure 16C). Moreover, the gel electrolytes were stable up to 310 °C, indicating that it has great applications in an extreme environment. On the other hand, Lin et al.[285] developed an ILs electrolyte by mixing *N*-methyl-*N*-propylpiperidinium bis(fluorosulfonyl)imide ($PIP_{13}FSI$) and *N*-butyl-*N*-methylpyrrolidinium bis(fluorosulfonyl)imide ($PYR_{14}FSI$) in a molar ratio of 1:1, which exhibited an operating temperature ranging from −50 °C to 100 °C. As presented in Figure 16D, the eutectic mixture formed by two ILs has a much lower melting point (−80 °C) than $PIP_{13}FSI$ (6 °C) and $PYR_{14}FSI$ (−18 °C). The SCs based on the mixed ionic liquid electrolytes and incorporated with nanostructured carbon electrodes showed a wide potential of 3.5 V and a wide operating range from −50 °C to 100 °C. The SCs based on the ILs gel-based electrolytes also exhibited an outstanding mechanical performance while keeping the good electrochemical performance. Shen et al.[286] reported flexible asymmetric SCs based on the FeOOH electrodes and the ILs electrolytes. The γ-FeOOH@carbon cloth, N-doped AC, and 1-ethyl-3-methylimidazolium bis(trifluoromethylsulfonyl) imide ($EMIM-NTF_2$)-fumed SiO_2 were used as the negative electrode, the positive electrode, and the electrolytes, respectively. Figure 16E illustrates the intercalation pseudocapacitance provided by $EMIM^+$ and FeOOH. The intercalation pseudocapacitance provided by $EMIM^+$ and FeOOH exhibited a promised electrochemical performance and the ($EMIM-NTF_2$)-fumed SiO_2 gel electrolytes could provide great stability. The SCs could exhibit the maximum energy density of 1.44 mWh/cm^3 at 200 °C and stable energy-storage ability at a 180° bending angle.

Recently, we reported novel ionic LGs composed of PVA, 1-butyl-3-methylimidazolium tetrafluoroborate (BMIMBF4), and tetrabutylammonium tetrafluoroborate

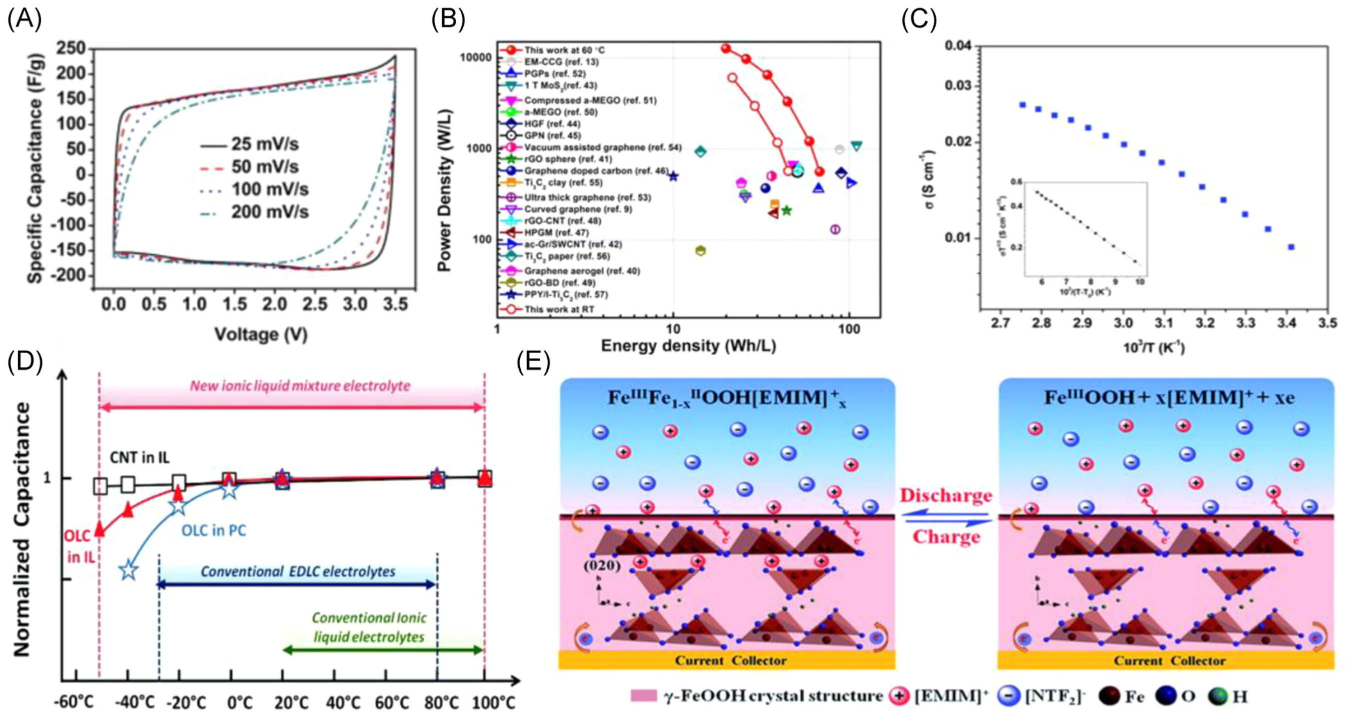

FIGURE 16 (A) The cyclic voltammetry curves of supercapacitor with graphene doped carbon materials and GO-EMIMBF4-[poly(vinylidene fluoride)-hexafluoro propylene (HFP)] ion gel as electrodes and electrolytes, respectively. Reproduced with permission: Copyright 2014, Elsevier.[282] (B) Ragone plot of supercapacitor with ionic liquid decorated graphene oxide and polypropylene (PP)-EMIMTFSI as electrodes and electrolyte, respectively. Reproduced with permission: Copyright 2017, American Chemical Society.[283] (C) The ionic conductivity of 1-ethyl-3-methylimidazolium tetracyanoborate (EMIMTCB) entrapped in poly(vinylidene fluoride-co-hexafluoropropylene) (PVdF-HFP) gel electrolytes. Reproduced with permission: Copyright 2013, Royal Society of Chemistry.[284] (D) The temperature range of the mixture of ($PIP_{13}FSI$) and ($PYR_{14}FSI$). Reproduced with permission: Copyright 2011, American Chemical Society.[285] (E) Schematic illustration of the intercalation pseudocapacitance provided by $EMIM^+$ and FeOOH. Reproduced with permission: Copyright 2016, Royal Society of Chemistry[286]

(TBABF4) (PVA:BMIMBF4:TBABF4) as the solid-state electrolytes, which exhibited dramatically enhanced ionic conductivity. Afterward, we demonstrated all-solid-state ASCs by using MnO_2 coated on carbon cloth (CC) as the positive electrode, rGO coated on a CC as the negative electrode, and PVA:$BMIMBF_4$:$TBABF_4$ gel as the solid-state electrolyte. Figure 17A schematically displays ASCs device configuration, MnO_2@CC//PVA:BMIMBF4:TBABF4//rGO@CC. ASCs exhibit a wide operational window from 0 to 3.0 V (Figure 17B). The ASCs possessed the highest specific capacitance of 49 F/g, the energy density of 61.2 Wh/kg, the power density of 1049 W/kg at the current density of 0.5 A/g (Figure 17C). Figure 17D displays the Ragone plot of MnO_2@CC//PVA:BMIMBF4:TBABF4//rGO@CC ASCs. Compared to the recently reported SCs incorporated with IL electrolytes, the MnO_2@CC//PVA:$BMIMBF_4$:$TBABF_4$//rGO@CC ASCs exhibited both high energy density and high power density. The ASCs maintained greater than 80% capacitance retention after the 3000 charge/discharge cycles at the current density of 3 A/g.[287]

4.4 | Double-network gel electrolytes

High energy density flexible all-solid-state SCs incorporated with hydrogel electrolytes (HEs) solid-state electrolytes have been reported.[250,288,289] However, the single-component solid-state HEs exhibited poor mechanical strength and flexibility.[250,288–290] To address these problems, solid-state double-network (DN) HEs, which are composed of two independent and interpenetrating polymer networks, have been developed for enhancing mechanical strength and flexibility.[243,291–299] The SCs with superior mechanical stretchability (up to 1000%) and excellent self-healing behavior under either heating or light treatment were reported by Li et al.,[243] where the SCs were incorporated with a multifunctional hydrogel polyelectrolyte with copolymerization of 2-acrylamido-2-methylpropane sulfonic acid and *N,N*-dimethylacrylamide. Lin et al.[291] reported a novel Li_2SO_4-containing agarose/polyacrylamide double-network (Li-AG/PAM DN) hydrogel electrolyte, which was synthesized by a heating-cooling and subsequent radiation-induced polymerization and cross-linking

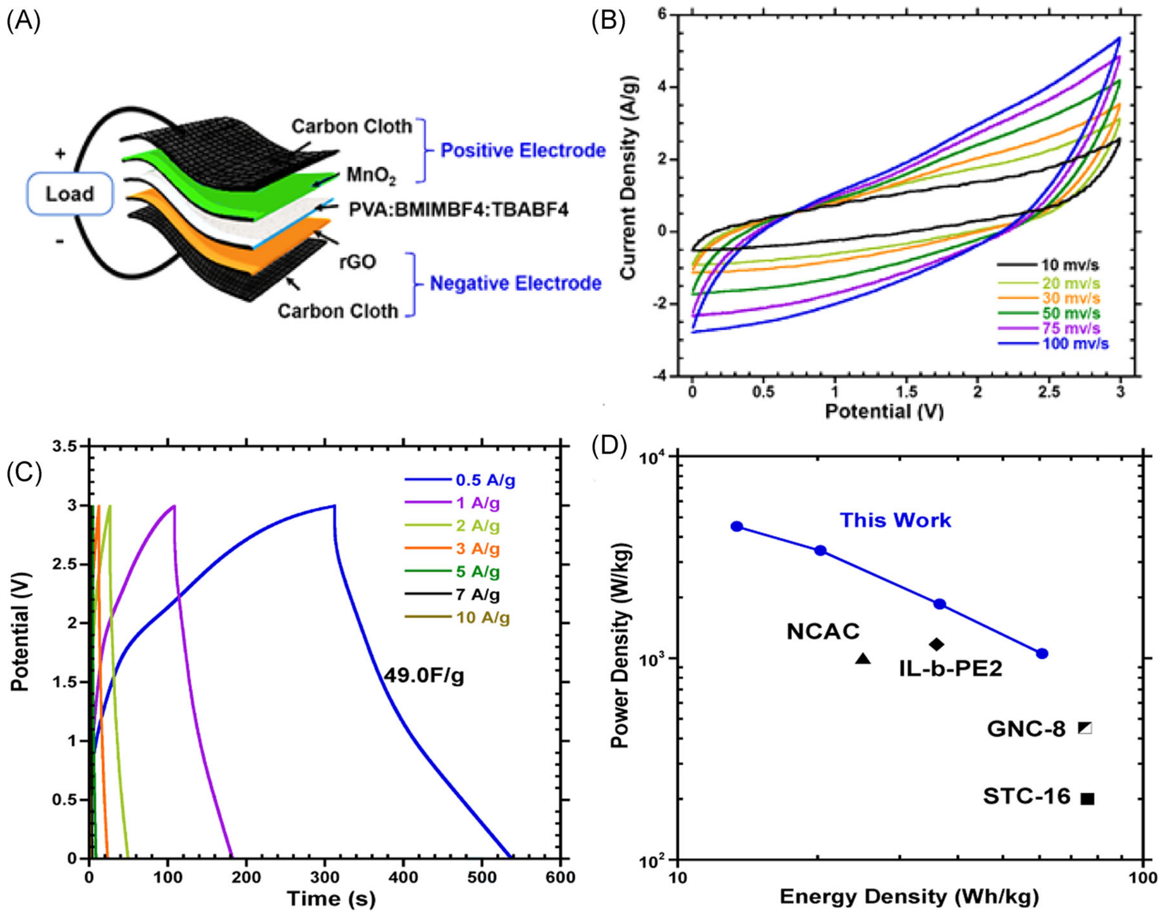

FIGURE 17 (A) Schematic illustration of asymmetric supercapacitors (ASCs) device configuration, (B) the cyclic voltammetry curves, (C) the galvanostatic charge-discharge curves, and (D) the Ragone plot of MnO_2@CC//polyvinyl alcohol:BMIMBF4:TBABF4//rGO@CC ASCs. Reproduced with permission: Copyright 2020, American Chemical Society[287]

process. The Li-AG/PAM DN hydrogel electrolyte possessed extremely excellent mechanical properties with a compression strength of 150 MPa, a fracture compression strain of above 99.9%, a tensile strength of 1103 kPa, and an elongation at a break of 2780%. They further demonstrated the flexible Li-AG/PAM DN hydrogel electrolyte-SC, which exhibited a low charge-transfer resistance, a good ionic diffusion, a superior rate capability, and good cycling stability, owing to the improved ionic transport in the Li-AG/PAM DN hydrogel electrolyte and electrode interfaces.[300] However, the solid-state DN HEs still possessed inferior energy densities.

Recently, we introduced Na_2MoO_4, a kind of pseudocapacitive redox additive into DN HEs.[226] The schematic illustration of the solid-state gelatin pHEAA chitosan Na_2MoO_4 DN HEs was shown in Figure 18A. Figure 18B presents the CV curves of the symtrical supercapacitors (SSCs) incorporated with the solid-state gelatin pHEAA chitosan Na_2MoO_4 DN HEs absorbed H_2SO_4 solution under different scan rates. All CV curves possess similar shapes in the operational window from 0 to 0.8 V, demonstrating that the SSCs incorporated with the solid-state gelatin pHEAA chitosan Na_2MoO_4 DN HEs absorbed H_2SO_4 solution have good reversible capacitive behaviors. The SSCs exhibit a specific capacitance of 84 mF/cm^2 (~420 F/g) at the current density of 1 mA/cm^2 (Figure 18C), which is three times that (28 mF/cm^2) from the SSCs incorporated with the solid-state gelatin pHEAA chitosan DN HEs absorbed H_2SO_4 solution at the same condition. A specific capacitance of 84 mF/cm^2 at the current density of 1 mA/cm^2 and a specific capacitance of 52% at the discharge current densities of 10 mA/cm^2 were observed (Figure 18D). The capacitance retention of SSCs is 62%, which is much higher than that (32%) of the SSCs incorporated with the solid-state gelatin pHEAA chitosan DN HEs absorbed H_2SO_4 solution. These results demonstrate that the SSCs incorporated with the solid-state gelatin pHEAA chitosan Na_2MoO_4 DN HEs are more stable than the electrochemical-double-layer capacitance provided by the interface between the electrodes and electrolytes at a higher current density. It was also found that the SSCs

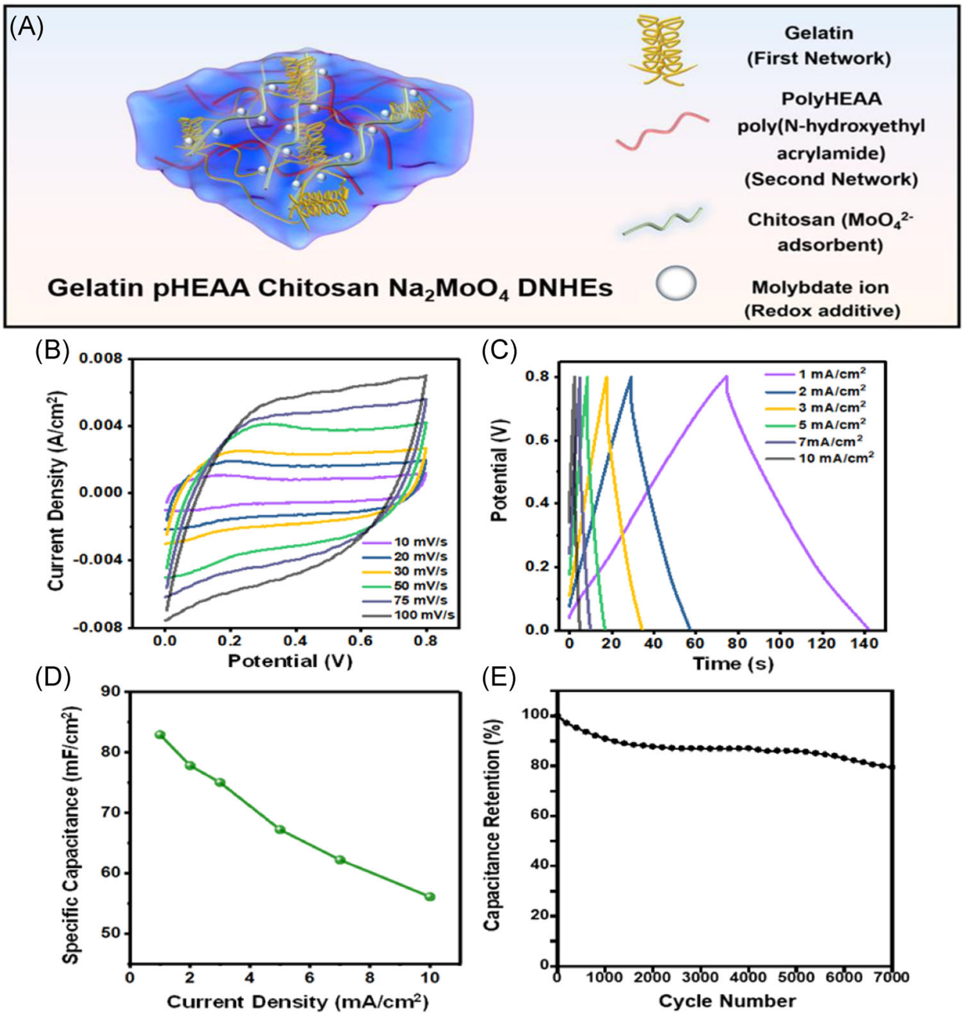

FIGURE 18 (A) Schematic illustration of the solid-state gelatin poly(*N*-hydroxyethyl acrylamide (pHEAA) chitosan Na_2MoO_4 double-network hydrogel electrolytes (solid-state gelatin pHEAA chitosan Na_2MoO_4 DN HEs), (B) the cyclic voltammetry curves of the active carbon cloth (ACC)//gelatin pHEAA chitosan Na_2MoO_4 DN HEs//ACC SSCs scanned at different rates, (C) the galvanostatic charge-discharge curves of the ACC//gelatin pHEAA chitosan Na_2MoO_4 DN HEs//ACC SSCs under different current densities, (D) the specific capacitance of the ACC//gelatin pHEAA chitosan Na_2MoO_4 DN hydrogel electrolytes//ACC SSCs under different charge/discharge current densities, (E) the cycling stability of the ACC//gelatin pHEAA chitosan Na_2MoO_4 DNHEs//ACC SSCs. SSC, symtrical supercapacitors. Reproduced with permission: Copyright 2021, American Chemical Society[226]

incorporated with the solid-state gelatin pHEAA chitosan Na_2MoO_4 DN HEs absorbed H_2SO_4 solution exhibited the energy density of ~34 Wh/kg at the power density of ~1800 W/kg, and the energy density of ~70 μWh/cm^2 at the power density of ~3800 μW/cm^2. These values are comparable to those reported recently. Figure 18E presents the cyclic stability of the SSCs. After 7000 charges/discharges cycles at the current density of 5 mA/cm^2, the SSCs can still retain approximately 80% of their initial capacitance. The decreased specific capacitance after 7000 charge/discharge cycles is probably originated from water evaporated from the solid-state gelatin pHEAA chitosan Na_2MoO_4 DN HEs, which could induce the solid-state gelatin pHEAA chitosan Na_2MoO_4 DN HEs detached from the ACC electrodes, resulting in poor ionic conductivity. Moreover, the SSCs possessed negligible degradation in both electrochemical performance and mechanical flexibility after they were bent 1000 times at 90° and retained approximately 80% capacitance retention after 7000 charge/discharge cycles, which indicated that the SSCs possessed excellent flexibility and stability.

5 | SUMMARY AND OUTLOOK

The solid-state SCs are playing more and more important roles in plenty of diverse energy storage systems, such as wearable electronics, self-powered devices, and smart medical devices. This review systemically introduced the basic mechanisms of different types of SCs and recent progress in both electrodes and electrolytes used for the development of solid-state flexible SCs. For the electrodes, except for the traditional carbon materials, conducting polymers, metal oxides, and other novel materials, such as metal nitrides, metal chalcogenides, MXenes, COFs, and MOFs, used for the electrodes were also overviewed. These emerging new materials have become promising candidates for approaching high-performance electrodes due to their unique electrochemical performance. For the electrolytes, polymer gel-based solid-state electrolytes have attracted more attention in both academia and industry sectors. The multicomponent polymeric matrices could provide both high mechanical and electrochemical performance for the flexible SCs. Moreover, solvent-free ionic liquids with large voltage and temperature windows could boost the high-energy-density devices and extend their applications in extreme situations.

Many impressive and encouraging methods have been developed for approaching high-performance flexible SCs, but the following challenges are needed to be addressed.

(1) The energy density of most flexible SCs was still lower than those in secondary batteries, which restricted the long-time endurance of the wearable and portable devices. Investigation of new pseudocapacitive materials with both high capacitance and large working windows is the primary objective.
(2) The emerging 2D layered materials, such as MXenes, transition metal nitrides, and chalcogenides have shown promising high-performance as the electrodes. However, the collapse between the individual layer with another one restricted the stability of these 2D materials, which have to be resolved.
(3) The understanding of ion transport dynamics in irregular porous structures is still lacking. Most reported mechanisms or simulations are based on the ideal model, which can not completely describe the real situation. With the help of in situ characterization, such as high-throughput synchrotron X-ray diffraction and absorbance, the more detailed mechanisms on charge transport and storage can provide clear insights on the design of new materials.
(4) Few studies focused on the interaction between the electrolyte ions and the polymeric matrices. The mechanisms of the influence of different polymer chains on ionic conductivity were still unclear. To explore the underlying of the polymeric chains in the matrices on the ionic conductivity probably could lead to a better understanding of further development of multicomponent polymeric matrices.
(5) In the past decades, most researchers described the device performance of SCs by the mass-specific capacitance. The mass to calculate the specific capacitance can be both the mass of active materials on electrodes and the whole devices. But for wearable and portable electronics, it is more reasonable to use the volumetric specific capacitance since these electronics are usually light. So the standard parameters should be set up to better describe the device performance.
(6) For the applications of SCs, the expensive electrode materials and low processability restrict the further developments of large-scale devices. Investigating the low cost and easily processable materials will benefit the developments of large-scale processing such as blade cast with roll-to-roll (R2R) processing.

ACKNOWLEDGMENT

The authors thank the National Science Foundation (No. ECCS/EPMD1903303) for financial support.

CONFLICTS OF INTEREST

The authors declare no conflicts of interest.

ORCID

Xiong Gong http://orcid.org/0000-0001-6525-3824

REFERENCES

1. Shao Y, El-Kady MF, Sun J, et al. Design and mechanisms of asymmetric supercapacitors. *Chem Rev*. 2018;118(18):9233-9280.
2. Dou Q, Wu N, Yuan H, et al. Emerging trends in anion storage materials for the capacitive and hybrid energy storage and beyond. *Chem Soc Rev*. 2021;50:6734-6789.
3. Yu M, Feng X. Thin-film electrode-based supercapacitors. *Joule*. 2019;3:338-360.
4. Yu G, Hu L, Vosgueritchian M, et al. Solution-processed graphene/MnO_2 nanostructured textiles for high-performance electrochemical capacitors. *Nano Lett*. 2011;11:2905-2911.
5. Liu C, Li F, Ma L-P, Cheng H-M. Advanced materials for energy storage. *Adv Mater*. 2010;22:E28-E62.
6. Liang J, Jiang C, Wu W. Printed flexible supercapacitor: ink formulation, printable electrode materials and applications. *Appl Phys Rev*. 2021;8:021319.
7. Simon P, Gogotsi Y. Materials for electrochemical capacitors. *Nat Mater*. 2008;7:845-854.
8. Sun H, Zhang Y, Zhang J, Sun X, Peng H. Energy harvesting and storage in 1D devices. *Nat Rev Mater*. 2017;2:17023.
9. Qi D, Liu Y, Liu Z, Zhang L, Chen X. Design of architectures and materials in in-plane micro-supercapacitors: current status and future challenges. *Adv Mater*. 2017;29:1602802.
10. Kusko A, Dedad J. Stored energy-short-term and long-term energy storage methods. *IEEE Ind Appl Mag*. 2007;13:66-72.
11. Kötz R, Carlen M. Principles and applications of electrochemical capacitors. *Electrochim Acta*. 2000;45:2483-2498.
12. Liang X, Long G, Fu C, et al. High performance all-solid-state flexible supercapacitor for wearable storage device application. *Chem Eng J*. 2018;345:186-195.

13. Jin X, Sun G, Yang H, et al. A graphene oxide-mediated polyelectrolyte with high ion-conductivity for highly stretchable and self-healing all-solid-state supercapacitors. *J Mater Chem A*. 2018;6:19463-19469.
14. Huang Y, Zhong M, Huang Y, et al. A self-healable and highly stretchable supercapacitor based on a dual crosslinked polyelectrolyte. *Nat Commun*. 2015;6:10310.
15. Dubal DP, Chodankar NR, Kim D-H, Gomez-Romero P. Towards flexible solid-state supercapacitors for smart and wearable electronics. *Chem Soc Rev*. 2018;47:2065-2129.
16. Yan C, Lee PS. Stretchable energy storage and conversion devices. *Small*. 2014;10:3443-3460.
17. Zhong C, Deng Y, Hu W, Qiao J, Zhang L, Zhang J. A review of electrolyte materials and compositions for electrochemical supercapacitors. *Chem Soc Rev*. 2015;44:7484-7539.
18. Shown I, Ganguly A, Chen L-C, Chen K-H. Conducting polymer-based flexible supercapacitor. *Energy Sci Eng*. 2015;3:2-26.
19. Yang P, Mai W. Flexible solid-state electrochemical supercapacitors. *Nano Energy*. 2014;8:274-290.
20. Béguin F, Presser V, Balducci A, Frackowiak E. Carbons and electrolytes for advanced supercapacitors. *Adv Mater*. 2014;26:2219-2251.
21. Helmholtz H. Ueber einige Gesetze der Vertheilung elektrischer Ströme in körperlichen Leitern mit Anwendung auf die thierisch-elektrischen Versuche. *Ann Phys*. 1853;165:211-233.
22. Gouy M. Sur la constitution de la charge électrique à la surface d'un électrolyte. *J Phys Theor Appl*. 1910;9:457-468.
23. Stern O. Zur theorie der elektrolytischen doppelschicht. *Zeitschrift für Elektrochemie und angewandte physikalische Chemie*. 1924;30:508-516.
24. Augustyn V, Simon P, Dunn B. Pseudocapacitive oxide materials for high-rate electrochemical energy storage. *Energ Environ Sci*. 2014;7:1597-1614.
25. Herrero E, Buller LJ, Abruña HD. Underpotential deposition at single crystal surfaces of Au, Pt, Ag and other materials. *Chem Rev*. 2001;101:1897-1930.
26. Dubal DP, Ayyad O, Ruiz V, Gómez-Romero P. Hybrid energy storage: the merging of battery and supercapacitor chemistries. *Chem Soc Rev*. 2015;44:1777-1790.
27. Sun X, Zhang X, Zhang H, Xu N, Wang K, Ma Y. High performance lithium-ion hybrid capacitors with pre-lithiated hard carbon anodes and bifunctional cathode electrodes. *J Power Sources*. 2014;270:318-325.
28. Thangavel R, Kaliyappan K, Kang K, Sun X, Lee Y-S. Going beyond lithium hybrid capacitors: proposing a new high-performing sodium hybrid capacitor system for next-generation hybrid vehicles made with bio-inspired activated carbon. *Adv Energy Mater*. 2016;6:1502199.
29. Wang X, Kajiyama S, Iinuma H, et al. Pseudocapacitance of MXene nanosheets for high-power sodium-ion hybrid capacitors. *Nat Commun*. 2015;6:6544.
30. Thangavel R, Moorthy B, Kim DK, Lee Y-S. Pushing the energy output and cyclability of sodium hybrid capacitors at high power to new limits. *Adv Energy Mater*. 2017;7:1602654.
31. Liu H, Liu X, Wang S, Liu H-K, Li L. Transition metal based battery-type electrodes in hybrid supercapacitors: a review. *Energy Stor Mater*. 2020;28:122-145.
32. Wang H, Xu Z, Li Z, et al. Hybrid device employing three-dimensional arrays of MnO in carbon nanosheets bridges battery—supercapacitor divide. *Nano Lett*. 2014;14:1987-1994.
33. Chen GZ. Supercapacitor and supercapattery as emerging electrochemical energy stores. *Int Mater Rev*. 2017;62:173-202.
34. Padmanathan N, Shao H, McNulty D, O'Dwyer C, Razeeb KM. Hierarchical $NiO\text{-}In_2O_3$ microflower (3D)/nanorod (1D) hetero-architecture as a supercapattery electrode with excellent cyclic stability. *J Mater Chem A*. 2016;4:4820-4830.
35. Shao H, Padmanathan N, McNulty D, O′Dwyer C, Razeeb KM. Supercapattery based on binder-free $Co_3(PO_4)_2{\cdot}8H_2O$ multilayer nano/microflakes on nickel foam. *ACS Appl Mater Interfaces*. 2016;8:28592-28598.
36. Sankar KV, Seo Y, Lee SC, et al. Cobalt carbonate hydroxides as advanced battery-type materials for supercapatteries: influence of morphology on performance. *Electrochim Acta*. 2018;259:1037-1044.
37. Amatucci GG, Badway F, Du Pasquier A, Zheng T. An asymmetric hybrid nonaqueous energy storage cell. *J Electrochem Soc*. 2001;148:A930.
38. Pasquier AD, Plitz I, Gural J, Menocal S, Amatucci G. Characteristics and performance of 500 F asymmetric hybrid advanced supercapacitor prototypes. *J Power Sources*. 2003;113:62-71.
39. Ni J, Yang L, Wang H, Gao L. A high-performance hybrid supercapacitor with $Li_4Ti_5O_{12}$-C nano-composite prepared by in situ and ex situ carbon modification. *J Solid State Electr*. 2012;16:2791-2796.
40. Sivakkumar SR, Nerkar JY, Pandolfo AG. Rate capability of graphite materials as negative electrodes in lithium-ion capacitors. *Electrochim Acta*. 2010;55:3330-3335.
41. Zhang X, Jiang C, Liang J, Wu W. Electrode materials and device architecture strategies for flexible supercapacitors in wearable energy storage. *J Mater Chem A*. 2021;9:8099-8128.
42. Frackowiak E, Delpeux S, Jurewicz K, Szostak K, Cazorla-Amoros D, Béguin F. Enhanced capacitance of carbon nanotubes through chemical activation. *Chem Phys Lett*. 2002;361:35-41.
43. Ruiz V, Blanco C, Raymundo-Piñero E, Khomenko V, Béguin F, Santamaría R. Effects of thermal treatment of activated carbon on the electrochemical behaviour in supercapacitors. *Electrochim Acta*. 2007;52:4969-4973.
44. Peng C, Zhang S, Jewell D, Chen GZ. Carbon nanotube and conducting polymer composites for supercapacitors. *Prog Nat Sci*. 2008;18:777-788.
45. Peng C, Jin J, Chen GZ. A comparative study on electrochemical co-deposition and capacitance of composite films of conducting polymers and carbon nanotubes. *Electrochim Acta*. 2007;53:525-537.
46. Yan J, Wei T, Cheng J, Fan Z, Zhang M. Preparation and electrochemical properties of lamellar MnO_2 for supercapacitors. *Mater Res Bull*. 2010;45:210-215.
47. Ahn YR, Song MY, Jo SM, Park CR, Kim DY. Electrochemical capacitors based on electrodeposited ruthenium oxide on nanofibre substrates. *Nanotechnology*. 2006;17:2865-2869.
48. Yan J, Ren CE, Maleski K, et al. Flexible MXene/graphene films for ultrafast supercapacitors with outstanding volumetric capacitance. *Adv Funct Mater*. 2017;27:1701264.

49. Sheberla D, Bachman JC, Elias JS, Sun CJ, Shao-Horn Y, Dincă M. Conductive MOF electrodes for stable supercapacitors with high areal capacitance. *Nat Mater*. 2017;16:220-224.
50. Wang P, Wu Q, Han L, et al. Synthesis of conjugated covalent organic frameworks/graphene composite for supercapacitor electrodes. *RSC Adv*. 2015;5:27290-27294.
51. Chhowalla M, Shin HS, Eda G, Li LJ, Loh KP, Zhang H. The chemistry of two-dimensional layered transition metal dichalcogenide nanosheets. *Nat Chem*. 2013;5:263-275.
52. Balamuralitharan B, Karthick SN, Balasingam SK, et al. Hybrid reduced graphene oxide/manganese diselenide cubes: a new electrode material for supercapacitors. *Energy Technol*. 2017;5:1953-1962.
53. Wang G, Zhang L, Zhang J. A review of electrode materials for electrochemical supercapacitors. *Chem Soc Rev*. 2012;41: 797-828.
54. Zhai T, Wang F, Yu M, et al. 3D MnO_2-graphene composites with large areal capacitance for high-performance asymmetric supercapacitors. *Nanoscale*. 2013;5:6790-6796.
55. Yu M, Huang Y, Li C, et al. Building three-dimensional graphene frameworks for energy storage and catalysis. *Adv Funct Mater*. 2015;25:324-330.
56. Wang G, Wang H, Lu X, et al. Solid-state supercapacitor based on activated carbon cloths exhibits excellent rate capability. *Adv Mater*. 2014;26:2676-2682.
57. Liu W, Yao Y, Fu O, et al. Lignin-derived carbon nanosheets for high-capacitance supercapacitors. *RSC Adv*. 2017;7:48537-48543.
58. Yu M, Zhang Y, Zeng Y, et al. Water surface assisted synthesis of large-scale carbon nanotube film for high-performance and stretchable supercapacitors. *Adv Mater*. 2014;26:4724-4729.
59. Borenstein A, Hanna O, Attias R, Luski S, Brousse T, Aurbach D. Carbon-based composite materials for supercapacitor electrodes: a review. *J Mater Chem A*. 2017;5:12653-12672.
60. Abioye AM, Ani FN. Recent development in the production of activated carbon electrodes from agricultural waste biomass for supercapacitors: a review. *Renew Sust Energ Rev*. 2015;52:1282-1293.
61. González A, Goikolea E, Barrena JA, Mysyk R. Review on supercapacitors: technologies and materials. *Renew Sust Energ Rev*. 2016;58:1189-1206.
62. Yao L, Wu Q, Zhang P, et al. Scalable 2D hierarchical porous carbon nanosheets for flexible supercapacitors with ultrahigh energy density. *Adv Mater*. 2018;30:1706054.
63. Zheng Q, Cai Z, Ma Z, Gong S. Cellulose nanofibril/reduced graphene oxide/carbon nanotube hybrid aerogels for highly flexible and all-solid-state supercapacitors. *ACS Appl Mater Interfaces*. 2015;7:3263-3271.
64. Xiong Z, Liao C, Han W, Wang X. Mechanically tough large-area hierarchical porous graphene films for high-performance flexible supercapacitor applications. *Adv Mater*. 2015;27:4469-4475.
65. Jiang L, Wang J, Mao X, et al. High rate performance carbon nano-cages with oxygen-containing functional groups as supercapacitor electrode materials. *Carbon*. 2017;111:207-214.
66. Chen Z, Zheng L, Zhu T, et al. All-solid-state flexible asymmetric supercapacitors fabricated by the binder-free hydrophilic carbon cloth@MnO_2 and hydrophilic carbon cloth@polypyrrole electrodes. *Adv Electron Mater*. 2019;5: 201800721.
67. Xia X, Zhang Y, Fan Z, et al. Novel metal@carbon spheres core-shell arrays by controlled self-assembly of carbon nanospheres: a stable and flexible supercapacitor electrode. *Adv Energy Mater*. 2015;5:1401709.
68. Li X, Tang Y, Song J, et al. Self-supporting activated carbon/carbon nanotube/reduced graphene oxide flexible electrode for high performance supercapacitor. *Carbon*. 2018;129:236-244.
69. Yao YM, Joo P, Jana SC. A surfactant-free microfluidic process for fabrication of multi-hollow polyimide aerogel particles. *Int Polym Process*. 2020;35:481-492.
70. Zhou Y, Wang X, Acauan L, et al. Ultrahigh-areal-capacitance flexible supercapacitor electrodes enabled by conformal P3MT on horizontally aligned carbon-nanotube arrays. *Adv Mater*. 2019;31:1901916.
71. Cheng X, Gui X, Lin Z, et al. Three-dimensional α-Fe_2O_3/carbon nanotube sponges as flexible supercapacitor electrodes. *J Mater Chem A*. 2015;3:20927-20934.
72. Chen Z, Yang Y, Ma Z, et al. All-solid-state asymmetric supercapacitors with metal selenides electrodes and ionic conductive composites electrolytes. *Adv Funct Mater*. 2019; 29:1904182.
73. Du P, Hu X, Yi C, et al. Self-powered electronics by integration of flexible solid-state graphene-based supercapacitors with high performance perovskite hybrid solar cells. *Adv Funct Mater*. 2015;25:2420-2427.
74. Zhu T, Yang Y, Liu Y, et al. Wireless portable light-weight self-charging power packs by perovskite-organic tandem solar cells integrated with solid-state asymmetric supercapacitors. *Nano Energy*. 2020;78:105397.
75. Yuksel R, Sarioba Z, Cirpan A, Hiralal P, Unalan HE. Transparent and flexible supercapacitors with single walled carbon nanotube thin film electrodes. *ACS Appl Mater Interfaces*. 2014;6:15434-15439.
76. Jiang S, Shi T, Zhan X, et al. High-performance all-solid-state flexible supercapacitors based on two-step activated carbon cloth. *J Power Sources*. 2014;272:16-23.
77. Zhao D, Chen C, Zhang Q, et al. High performance, flexible, solid-state supercapacitors based on a renewable and biodegradable mesoporous cellulose membrane. *Adv Energy Mater*. 2017;7:1700739.
78. Chen T, Dai L. Flexible and wearable wire-shaped micro-supercapacitors based on highly aligned titania and carbon nanotubes. *Energy Stor Mater*. 2016;2:21-26.
79. Parvez K, Wu Z-S, Li R, et al. Exfoliation of graphite into graphene in aqueous solutions of inorganic salts. *J Am Chem Soc*. 2014;136:6083-6091.
80. Yun J, Kim D, Lee G, Ha JS. All-solid-state flexible micro-supercapacitor arrays with patterned graphene/MWNT electrodes. *Carbon*. 2014;79:156-164.
81. Kang YJ, Chung H, Kim M-S, Kim W. Enhancement of CNT/PET film adhesion by nano-scale modification for flexible all-solid-state supercapacitors. *Appl Surf Sci*. 2015;355:160-165.
82. Liu S, Xie J, Li H, et al. Nitrogen-doped reduced graphene oxide for high-performance flexible all-solid-state micro-supercapacitors. *J Mater Chem A*. 2014;2:18125-18131.

83. Fan X, Chen T, Dai L. Graphene networks for high-performance flexible and transparent supercapacitors. *RSC Adv*. 2014;4:36996-37002.
84. Wang H, Deng J, Xu C, et al. Ultramicroporous carbon cloth for flexible energy storage with high areal capacitance. *Energy Stor Mater*. 2017;7:216-221.
85. Ramadoss A, Yoon K-Y, Kwak M-J, Kim SI, Ryu ST, Jang JH. Fully flexible, lightweight, high performance all-solid-state supercapacitor based on 3-dimensional-graphene/graphite-paper. *J Power Sources*. 2017;337:159-165.
86. Liu L, Ye D, Yu Y, Liu L, Wu Y. Carbon-based flexible micro-supercapacitor fabrication via mask-free ambient micro-plasma-jet etching. *Carbon*. 2017;111:121-127.
87. Song L, Cao X, Li L, et al. General method for large-area films of carbon nanomaterials and application of a self-assembled carbon nanotube film as a high-performance electrode material for an all-solid-state supercapacitor. *Adv Funct Mater*. 2017;27:1700474.
88. Li H-Y, Yu Y, Liu L, Liu L, Wu Y. One-step electrochemically expanded graphite foil for flexible all-solid supercapacitor with high rate performance. *Electrochim Acta*. 2017;228:553-561.
89. Li N, Huang X, Zhang H, Li Y, Wang C. Transparent and self-supporting graphene films with wrinkled- graphene-wall-assembled opening polyhedron building blocks for high performance flexible/transparent supercapacitors. *ACS Appl Mater Interfaces*. 2017;9:9763-9771.
90. Prasad KR, Koga K, Miura N. Electrochemical deposition of nanostructured indium oxide: high-performance electrode material for redox supercapacitors. *Chem Mater*. 2004;16:1845-1847.
91. Gupta V, Miura N. High performance electrochemical supercapacitor from electrochemically synthesized nanostructured polyaniline. *Mater Lett*. 2006;60:1466-1469.
92. Meng Q, Cai K, Chen Y, Chen L. Research progress on conducting polymer based supercapacitor electrode materials. *Nano Energy*. 2017;36:268-285.
93. Conway BE. *Electrochemical Supercapacitors: Scientific Fundamentals and Technological Applications*. Springer Science & Business; 2013.
94. Sharma P, Bhatti TS. A review on electrochemical double-layer capacitors. *Energy Convers Manag*. 2010;51:2901-2912.
95. Lu X-F, Chen X-Y, Zhou W, Tong Y-X, Li G-R. α-Fe_2O_3@PANI core-shell nanowire arrays as negative electrodes for asymmetric supercapacitors. *ACS Appl Mater Interfaces*. 2015;7:14843-14850.
96. Ren L, Zhang G, Yan Z, et al. Three-dimensional tubular MoS_2/PANI hybrid electrode for high rate performance supercapacitor. *ACS Appl Mater Interfaces*. 2015;7:28294-28302.
97. Huang Y, Li H, Wang Z, et al. Nanostructured polypyrrole as a flexible electrode material of supercapacitor. *Nano Energy*. 2016;22:422-438.
98. Ambade RB, Ambade SB, Shrestha NK, et al. Polythiophene infiltrated TiO_2 nanotubes as high-performance supercapacitor electrodes. *Chem Commun*. 2013;49:2308-2310.
99. Zhou G, Yuan T, Cai L, et al. Highly stable transparent conductive silver grid/PEDOT: PSS electrodes for integrated bifunctional flexible electrochromic supercapacitors. *Adv Energy Mater*. 2016;6:1501882.
100. Lei C, Wilson P, Lekakou C. Effect of poly(3,4-ethylenedioxythiophene) (PEDOT) in carbon-based composite electrodes for electrochemical supercapacitors. *J Power Sources*. 2011;196:7823-7827.
101. Peng X, Huo K, Fu J, Zhang X, Gao B, Chu PK. Coaxial PANI/TiN/PANI nanotube arrays for high-performance supercapacitor electrodes. *Chem Commun*. 2013;49:10172-10174.
102. Zhang J, Jiang J, Li H, Zhao XS. A high-performance asymmetric supercapacitor fabricated with graphene-based electrodes. *Energy Environ Sci*. 2011;4:4009-4015.
103. Li L, Lou Z, Han W, Chen D, Jiang K, Shen G. Highly stretchable micro-supercapacitor arrays with hybrid MWCNT/PANI electrodes. *Adv Mater Technol*. 2017;2:1600282.
104. Zang X, Li X, Zhu M, et al. Graphene/polyaniline woven fabric composite films as flexible supercapacitor electrodes. *Nanoscale*. 2015;7:7318-7322.
105. Chen W, Xia C, Alshareef HN. Graphene based integrated tandem supercapacitors fabricated directly on separators. *Nano Energy*. 2015;15:1-8.
106. Zhao D, Zhang Q, Chen W, et al. Highly flexible and conductive cellulose-mediated PEDOT: PSS/MWCNT composite films for supercapacitor electrodes. *ACS Appl Mater Interfaces*. 2017;9:13213-13222.
107. Anothumakkool B, Soni R, Bhange SN, Kurungot S. Novel scalable synthesis of highly conducting and robust PEDOT paper for a high performance flexible solid supercapacitor. *Energy Environ Sci*. 2015;8:1339-1347.
108. Li W, Guo Y, Wang Y, et al. A "chain–lock" strategy to construct a conjugated copolymer network for supercapacitor applications. *J Mater Chem A*. 2019;7:116-123.
109. Liu Z, Li Z, Cai Z, et al. Vapor-induced marangoni coating for organic functional films. *J Mater Chem C*. 2021;9:17518-17525.
110. Fan X, Nie W, Tsai H, et al. PEDOT: PSS for flexible and stretchable electronics: modifications, strategies, and applications. *Adv Sci*. 2019;6:1900813.
111. Zhu T, Yang Y, Zheng L, Liu L, Becker ML, Gong X. Solution-processed flexible broadband photodetectors with solution-processed transparent polymeric electrode. *Adv Funct Mater*. 2020;30:1909487.
112. Liu X, Qian T, Xu N, Zhou J, Guo J, Yan C. Preparation of on chip, flexible supercapacitor with high performance based on electrophoretic deposition of reduced graphene oxide/polypyrrole composites. *Carbon*. 2015;92:348-353.
113. Chen Y, Cai K, Liu C, Song H, Yang X. High-performance and breathable polypyrrole coated air-laid paper for flexible all-solid-state supercapacitors. *Adv Energy Mater*. 2017;7:1701247.
114. Li H, Song J, Wang L, et al. Flexible all-solid-state supercapacitors based on polyaniline orderly nanotubes array. *Nanoscale*. 2017;9:193-200.
115. Chen F, Wan P, Xu H, Sun X. Flexible transparent supercapacitors based on hierarchical nanocomposite films. *ACS Appl Mater Interfaces*. 2017;9:17865-17871.
116. Yao B, Wang H, Zhou Q, et al. Ultrahigh-conductivity polymer hydrogels with arbitrary structures. *Adv Mater*. 2017;29:1700974.

117. Wan C, Jiao Y, Li J. Flexible, highly conductive, and free-standing reduced graphene oxide/polypyrrole/cellulose hybrid papers for supercapacitor electrodes. *J Mater Chem A*. 2017;5:3819-3831.
118. Zhao D-D, Bao S-J, Zhou W-J, Li H-L. Preparation of hexagonal nanoporous nickel hydroxide film and its application for electrochemical capacitor. *Electrochem Commun*. 2007;9:869-874.
119. Jiang H, Ma J, Li C. Mesoporous carbon incorporated metal oxide nanomaterials as supercapacitor electrodes. *Adv Mater*. 2012;24:4197-4202.
120. Sk MM, Yue CY, Ghosh K, Jena RK. Review on advances in porous nanostructured nickel oxides and their composite electrodes for high-performance supercapacitors. *J Power Sources*. 2016;308:121-140.
121. Warren R, Sammoura F, Tounsi F, Sanghadasa M, Lin L. Highly active ruthenium oxide coating via ALD and electrochemical activation in supercapacitor applications. *J Mater Chem A*. 2015;3:15568-15575.
122. Wang X, Yin Y, Hao C, You Z. A high-performance three-dimensional micro supercapacitor based on ripple-like ruthenium oxide-carbon nanotube composite films. *Carbon*. 2015;82:436-445.
123. Muniraj VKA, Kamaja CK, Shelke MV. $RuO_2 \cdot nH_2O$ nanoparticles anchored on carbon nano-onions: an efficient electrode for solid state flexible electrochemical supercapacitor. *ACS Sustain Chem Eng*. 2016;4:2528-2534.
124. Ansari SA, Parveen N, Han TH, Ansari MO, Cho MH. Fibrous polyaniline@manganese oxide nanocomposites as supercapacitor electrode materials and cathode catalysts for improved power production in microbial fuel cells. *Phys Chem Chem Phys*. 2016;18:9053-9060.
125. Wang M, Li Z, Wang C, et al. Novel core-shell FeOF/$Ni(OH)_2$ hierarchical nanostructure for all-solid-state flexible supercapacitors with enhanced performance. *Adv Funct Mater*. 2017;27:1701014.
126. Lv Z, Luo Y, Tang Y, et al. Editable supercapacitors with customizable stretchability based on mechanically strengthened ultralong MnO_2 nanowire composite. *Adv Mater*. 2018;30:1704531.
127. Guan C, Liu X, Ren W, Li X, Cheng C, Wang J. Rational design of metal-organic framework derived hollow $NiCo_2O_4$ arrays for flexible supercapacitor and electrocatalysis. *Adv Energy Mater*. 2017;7:1602391.
128. Foo CY, Sumboja A, Tan DJH, Wang J, Lee PS. Flexible and highly scalable V_2O_5-rGO electrodes in an organic electrolyte for supercapacitor devices. *Adv Energy Mater*. 2014;4:1400236.
129. Yang P, Chao D, Zhu C, et al. Ultrafast-charging supercapacitors based on corn-like titanium nitride nanostructures. *Adv Sci*. 2016;3:1500299.
130. Acerce M, Voiry D, Chhowalla M. Metallic 1T phase MoS_2 nanosheets as supercapacitor electrode materials. *Nat Nanotechnol*. 2015;10:313-318.
131. Fan LZ, Hu YS, Maier J, Adelhelm P, Smarsly B, Antonietti M. High electroactivity of polyaniline in supercapacitors by using a hierarchically porous carbon monolith as a support. *Adv Funct Mater*. 2007;17:3083-3087.
132. Chang J-K, Lee M-T, Tsai W-T. In situ Mn K-edge X-ray absorption spectroscopic studies of anodically deposited manganese oxide with relevance to supercapacitor applications. *J Power Sources*. 2007;166:590-594.
133. Toupin M, Brousse T, Bélanger D. Influence of microstucture on the charge storage properties of chemically synthesized manganese dioxide. *Chem Mater*. 2002;14:3946-3952.
134. Toupin M, Brousse T, Bélanger D. Charge storage mechanism of MnO_2 electrode used in aqueous electrochemical capacitor. *Chem Mater*. 2004;16:3184-3190.
135. Shen H, Zhang Y, Song X, et al. Facile hydrothermal synthesis of actiniaria-shaped α-MnO_2/activated carbon and its electrochemical performances of supercapacitor. *J Alloy Compd*. 2019;770:926-933.
136. Radhamani AV, Shareef KM, Rao MSR. ZnO@MnO_2 core-shell nanofiber cathodes for high performance asymmetric supercapacitors. *ACS Appl Mater Interfaces*. 2016;8:30531-30542.
137. Shi P, Li L, Hua L, et al. Design of amorphous manganese oxide@multiwalled carbon nanotube fiber for robust solid-state supercapacitor. *ACS Nano*. 2017;11:444-452.
138. Dey MK, Sahoo PK, Satpati AK. Electrochemically deposited layered MnO_2 films for improved supercapacitor. *J Electroanal Chem*. 2017;788:175-183.
139. Choi C, Sim HJ, Spinks GM, Lepró X, Baughman RH, Kim SJ. Elastomeric and dynamic MnO_2/CNT core-shell structure coiled yarn supercapacitor. *Adv Energy Mater*. 2016;6:1502119.
140. Huang Z-H, Song Y, Feng D-Y, Sun Z, Sun X, Liu XX. High mass loading MnO_2 with hierarchical nanostructures for supercapacitors. *ACS Nano*. 2018;12:3557-3567.
141. Yan J, Fan Z, Sun W, et al. Advanced asymmetric supercapacitors based on $Ni(OH)_2$/graphene and porous graphene electrodes with high energy density. *Adv Funct Mater*. 2012;22:2632-2641.
142. Ji J, Zhang LL, Ji H, et al. Nanoporous $Ni(OH)_2$ thin film on 3D ultrathin-graphite foam for asymmetric supercapacitor. *ACS Nano*. 2013;7:6237-6243.
143. Li J, Zhao W, Huang F, Manivannan A, Wu N. Single-crystalline $Ni(OH)_2$ and NiO nanoplatelet arrays as supercapacitor electrodes. *Nanoscale*. 2011;3:5103-5109.
144. Jayashree RS, Vishnu KP. Suppression of the α-β-nickel hydroxide transformation in concentrated alkali: role of dissolved cations. *J Appl Electrochem*. 2001;31:1315-1320.
145. Lu X, Yu M, Zhai T, et al. High energy density asymmetric quasi-solid-state supercapacitor based on porous vanadium nitride nanowire anode. *Nano Lett*. 2013;13:2628-2633.
146. Zhu J, Cao L, Wu Y, et al. Building 3D structures of vanadium pentoxide nanosheets and application as electrodes in supercapacitors. *Nano Lett*. 2013;13:5408-5413.
147. Yan Y, Li B, Guo W, Pang H, Xue H. Vanadium based materials as electrode materials for high performance supercapacitors. *J Power Sources*. 2016;329:148-169.
148. Perera SD, Patel B, Nijem N, et al. Vanadium oxide nanowire-carbon nanotube binder-free flexible electrodes for supercapacitors. *Adv Energy Mater*. 2011;1:936-945.
149. Ghimbeu CM, Raymundo-Piñero E, Fioux P, Béguin F, Vix-Guterl C. Vanadium nitride/carbon nanotube nanocomposites as electrodes for supercapacitors. *J Mater Chem*. 2011;21:13268-13275.

150. Perera SD, Liyanage AD, Nijem N, Ferraris JP, Chabal YJ, Balkus KJ. Vanadium oxide nanowire-graphene binder free nanocomposite paper electrodes for supercapacitors: a facile green approach. *J Power Sources*. 2013;230:130-137.
151. Boukhalfa S, Evanoff K, Yushin G. Atomic layer deposition of vanadium oxide on carbon nanotubes for high-power supercapacitor electrodes. *Energ Environ Sci*. 2012;5:6872-6879.
152. Li R, Wang Y, Zhou C, et al. Carbon-stabilized high-capacity ferroferric oxide nanorod array for flexible solid-state alkaline battery-supercapacitor hybrid device with high environmental suitability. *Adv Funct Mater*. 2015;25:5384-5394.
153. Muralidharan N, Westover AS, Sun H, et al. From the junkyard to the power grid: ambient processing of scrap metals into nanostructured electrodes for ultrafast rechargeable batteries. *ACS Energy Lett*. 2016;1:1034-1041.
154. Sarkar D, Shukla A, Sarma DD. Substrate integrated nickel–iron ultrabattery with extraordinarily enhanced performances. *ACS Energy Lett*. 2016;1:82-88.
155. Lu X, Liu T, Zhai T, et al. Improving the cycling stability of metal-nitride supercapacitor electrodes with a thin carbon shell. *Adv Energy Mater*. 2014;4:1300994.
156. Wang S, Zhang L, Sun C, et al. Gallium nitride crystals: novel supercapacitor electrode materials. *Adv Mater*. 2016;28:3768-3776.
157. Cui H, Zhu G, Liu X, et al. Niobium nitride Nb_4N_5 as a new high-performance electrode material for supercapacitors. *Adv Sci*. 2015;2:1500126.
158. Huang H, Cui J, Liu G, Bi R, Zhang L. Carbon-coated $MoSe_2$/MXene hybrid nanosheets for superior potassium storage. *ACS Nano*. 2019;13:3448-3456.
159. Zhao X, Cai W, Yang Y, et al. $MoSe_2$ nanosheets perpendicularly grown on graphene with Mo-C bonding for sodium-ion capacitors. *Nano Energy*. 2018;47:224-234.
160. Shen Q, Jiang P, He H, Chen C, Liu Y, Zhang M. Encapsulation of $MoSe_2$ in carbon fibers as anodes for potassium ion batteries and nonaqueous battery-supercapacitor hybrid devices. *Nanoscale*. 2019;11:13511-13520.
161. Xie X, Makaryan T, Zhao M, Van Aken KL, Gogotsi Y, Wang G. MoS_2 nanosheets vertically aligned on carbon paper: a freestanding electrode for highly reversible sodium-ion batteries. *Adv Energy Mater*. 2016;6:1502161.
162. Zhang X, Xie Y. Recent advances in free-standing two-dimensional crystals with atomic thickness: design, assembly and transfer strategies. *Chem Soc Rev*. 2013;42:8187-8199.
163. Wang S, Guan BY, Yu L, Lou XW. Rational design of three-layered TiO_2@carbon@MoS_2 hierarchical nanotubes for enhanced lithium storage. *Adv Mater*. 2017;29:1702724.
164. Peng H, Wei C, Wang K, et al. $Ni_{0.85}Se$@$MoSe_2$ nanosheet arrays as the electrode for high-performance supercapacitors. *ACS Appl Mater Interfaces*. 2017;9:17067-17075.
165. Liang J, Tian B, Li S, Jiang C, Wu W. All-printed MnHCF-MnO_x-based high-performance flexible supercapacitors. *Adv Energy Mater*. 2020;10:2000022.
166. Zheng Y, Lin Z, Chen W, et al. Flexible, sandwich-like CNTs/$NiCo_2O_4$ hybrid paper electrodes for all-solid state supercapacitors. *J Mater Chem A*. 2017;5:5886-5894.
167. Li Y, Wang X, Yang Q, et al. Ultra-fine CuO nanoparticles embedded in three-dimensional graphene network nanostructure for high-performance flexible supercapacitors. *Electrochim Acta*. 2017;234:63-70.
168. Li N, Lv T, Yao Y, Li H, Liu K, Chen T. Compact graphene/MoS_2 composite films for highly flexible and stretchable all-solid-state supercapacitors. *J Mater Chem A*. 2017;5:3267-3273.
169. Naguib M, Kurtoglu M, Presser V, et al. Two-dimensional nanocrystals produced by exfoliation of Ti_3AlC_2. *Adv Mater*. 2011;23:4248-4253.
170. Anasori B, Xie Y, Beidaghi M, et al. Two-dimensional, ordered, double transition metals carbides (MXenes). *ACS Nano*. 2015;9:9507-9516.
171. Ghidiu M, Naguib M, Shi C, et al. Synthesis and characterization of two-dimensional Nb_4C_3 (MXene). *Chem Commun*. 2014;50:9517-9520.
172. Gogotsi Y. Transition metal carbides go 2D. *Nat Mater*. 2015;14:1079-1080.
173. Khazaei M, Arai M, Sasaki T, et al. Novel electronic and magnetic properties of two-dimensional transition metal carbides and nitrides. *Adv Funct Mater*. 2013;23:2185-2192.
174. Naguib M, Halim J, Lu J, et al. New two-dimensional niobium and vanadium carbides as promising materials for Li-ion batteries. *J Am Chem Soc*. 2013;135:15966-15969.
175. Naguib M, Mashtalir O, Carle J, et al. Two-dimensional transition metal carbides. *ACS Nano*. 2012;6:1322-1331.
176. Naguib M, Mochalin VN, Barsoum MW, Gogotsi Y. 25th Anniversary article: MXenes: a new family of two-dimensional materials. *Adv Mater*. 2014;26:992-1005.
177. Ghidiu M, Lukatskaya MR, Zhao M-Q, Gogotsi Y, Barsoum MW. Conductive two-dimensional titanium carbide 'clay' with high volumetric capacitance. *Nature*. 2014;516:78-81.
178. Liu G, Shen J, Ji Y, et al. Two-dimensional Ti_2CT_x MXene membranes with integrated and ordered nanochannels for efficient solvent dehydration. *J Mater Chem A*. 2019;7:12095-12104.
179. Zhao J, Zhang L, Xie X-Y, et al. $Ti_3C_2T_x$ (T = F, OH) MXene nanosheets: conductive 2D catalysts for ambient electrohydrogenation of N_2 to NH_3. *J Mater Chem A*. 2018;6:24031-24035.
180. Zhang CJ, Anasori B, Seral-Ascaso A, et al. Transparent, flexible, and conductive 2D titanium carbide (MXene) films with high volumetric capacitance. *Adv Mater*. 2017;29:1702678.
181. Zhu M, Huang Y, Deng Q, et al. Highly flexible, freestanding supercapacitor electrode with enhanced performance obtained by hybridizing polypyrrole chains with MXene. *Adv Energy Mater*. 2016;6:1600969.
182. Shahzad F, Alhabeb M, Hatter CB, et al. Electromagnetic interference shielding with 2D transition metal carbides (MXenes). *Science*. 2016;353:1137-1140.
183. Lipatov A, Alhabeb M, Lukatskaya MR, Boson A, Gogotsi Y, Sinitskii A. Effect of synthesis on quality, electronic properties and environmental stability of individual monolayer Ti_3C_2 MXene flakes. *Adv Electron Mater*. 2016;2:1600255.

184. Lukatskaya MR, Mashtalir O, Ren CE, et al. Cation intercalation and high volumetric capacitance of two-dimensional titanium carbide. *Science*. 2013;341:1502-1505.
185. Mashtalir O, Naguib M, Mochalin VN, et al. Intercalation and delamination of layered carbides and carbonitrides. *Nat Commun*. 2013;4:1716.
186. Mashtalir O, Lukatskaya MR, Zhao M-Q, Barsoum MW, Gogotsi Y. Amine-assisted delamination of Nb_2C MXene for Li-ion energy storage devices. *Adv Mater*. 2015;27:3501-3506.
187. Naguib M, Unocic RR, Armstrong BL, Nanda J. Large-scale delamination of multi-layers transition metal carbides and carbonitrides "MXenes". *Dalton Trans*. 2015;44:9353-9358.
188. Anasori B, Lukatskaya MR, Gogotsi Y. 2D metal carbides and nitrides (MXenes) for energy storage. *Nat Rev Mater*. 2017;2:16098.
189. Wen Y, Rufford TE, Chen X, et al. Nitrogen-doped $Ti_3C_2T_x$ MXene electrodes for high-performance supercapacitors. *Nano Energy*. 2017;38:368-376.
190. Jiang Q, Kurra N, Alhabeb M, Gogotsi Y, Alshareef HN. All pseudocapacitive MXene-RuO_2 asymmetric supercapacitors. *Adv Energy Mater*. 2018;8:1703043.
191. Li H, Hou Y, Wang F, et al. Flexible all-solid-state supercapacitors with high volumetric capacitances boosted by solution processable MXene and electrochemically exfoliated graphene. *Adv Energy Mater*. 2017;7:1601847.
192. Salunkhe RR, Kaneti YV, Kim J, Kim JH, Yamauchi Y. Nanoarchitectures for metal-organic framework-derived nanoporous carbons toward supercapacitor applications. *Acc Chem Res*. 2016;49:2796-2806.
193. Salunkhe RR, Kaneti YV, Yamauchi Y. Metal-organic framework-derived nanoporous metal oxides toward supercapacitor applications: progress and prospects. *ACS Nano*. 2017;11:5293-5308.
194. Xuan W, Zhu C, Liu Y, Cui Y. Mesoporous metal-organic framework materials. *Chem Soc Rev*. 2012;41:1677-1695.
195. Yaghi OM, Li H. Hydrothermal synthesis of a metal-organic framework containing large rectangular channels. *J Am Chem Soc*. 1995;117:10401-10402.
196. Choi KM, Jeong HM, Park JH, Zhang YB, Kang JK, Yaghi OM. Supercapacitors of nanocrystalline metal-organic frameworks. *ACS Nano*. 2014;8:7451-7457.
197. Salunkhe RR, Tang J, Kamachi Y, Nakato T, Kim JH, Yamauchi Y. Asymmetric supercapacitors using 3D nanoporous carbon and cobalt oxide electrodes synthesized from a single metal-organic framework. *ACS Nano*. 2015;9:6288-6296.
198. Khayum M A, Vijayakumar V, Karak S, et al. Convergent covalent organic framework thin sheets as flexible supercapacitor electrodes. *ACS Appl Mater Interfaces*. 2018;10:28139-28146.
199. Jiang Z, Li Z, Qin Z, Sun H, Jiao X, Chen D. LDH nanocages synthesized with MOF templates and their high performance as supercapacitors. *Nanoscale*. 2013;5:11770-11775.
200. Meng F, Fang Z, Li Z, et al. Porous Co_3O_4 materials prepared by solid-state thermolysis of a novel Co-MOF crystal and their superior energy storage performances for supercapacitors. *J Mater Chem A*. 2013;1:7235-7241.
201. Wang F, Wu X, Yuan X, et al. Latest advances in supercapacitors: from new electrode materials to novel device designs. *Chem Soc Rev*. 2017;46:6816-6854.
202. Khattak AM, Ghazi ZA, Liang B, et al. A redox-active 2D covalent organic framework with pyridine moieties capable of faradaic energy storage. *J Mater Chem A*. 2016;4:16312-16317.
203. Ding S-Y, Wang W. Covalent organic frameworks (COFs): from design to applications. *Chem Soc Rev*. 2013;42:548-568.
204. Côté AP, Benin AI, Ockwig NW, O'Keeffe M, Matzger AJ, Yaghi OM. Porous, crystalline, covalent organic frameworks. *Science*. 2005;310:1166-1170.
205. DeBlase CR, Silberstein KE, Truong T-T, Abruña HD, Dichtel WR. β-ketoenamine-linked covalent organic frameworks capable of pseudocapacitive energy storage. *J Am Chem Soc*. 2013;135:16821-16824.
206. Wang X, Liu B, Liu R, et al. Fiber-based flexible all-solid-state asymmetric supercapacitors for integrated photodetecting system. *Angew Chem Int Ed*. 2014;53:1849-1853.
207. Cao X, Zheng B, Shi W, et al. Reduced graphene oxide-wrapped MoO_3 composites prepared by using metal-organic frameworks as precursor for all-solid-state flexible supercapacitors. *Adv Mater*. 2015;27:4695-4701.
208. Cheng T, Zhang Y-Z, Zhang J-D, Lai W-Y, Huang W. High-performance free-standing PEDOT: PSS electrodes for flexible and transparent all-solid-state supercapacitors. *J Mater Chem A*. 2016;4:10493-10499.
209. Xu T, Ding X, Liang Y, Zhao Y, Chen N, Qu L. Direct spinning of fiber supercapacitor. *Nanoscale*. 2016;8:12113-12117.
210. Lu C, Wang D, Zhao J, Han S, Chen W. A continuous carbon nitride polyhedron assembly for high-performance flexible supercapacitors. *Adv Funct Mater*. 2017;27:1606219.
211. Westover AS, Tian JW, Bernath S, et al. A multifunctional load-bearing solid-state supercapacitor. *Nano Lett*. 2014;14:3197-3202.
212. Lu C, Chen X. In situ synthesized PEO/NBR composite ionogels for high-performance all-solid-state supercapacitors. *Chem Commun*. 2019;55:8470-8473.
213. Huang Y, Zhong M, Shi F, et al. An intrinsically stretchable and compressible supercapacitor containing a polyacrylamide hydrogel electrolyte. *Angew Chem Int Ed*. 2017;56:9141-9145.
214. Li L, Lu F, Wang C, et al. Flexible double-cross-linked cellulose-based hydrogel and aerogel membrane for supercapacitor separator. *J Mater Chem A*. 2018;6:24468-24478.
215. Chen C-M, Zhang Q, Huang C-H, et al. Macroporous 'bubble' graphene film via template-directed ordered-assembly for high rate supercapacitors. *Chem Commun*. 2012;48:7149-7151.
216. Hahm MG, Leela Mohana Reddy A, Cole DP, et al. Carbon nanotube-nanocup hybrid structures for high power supercapacitor applications. *Nano Lett*. 2012;12:5616-5621.
217. Hou G-M, Huang Y-F, Ruan W-H, Zhang M-Q, Rong M-Z. Hypergrafted nano-silica modified polymer gel electrolyte for high-performance solid-state supercapacitor. *J Solid State Electr*. 2016;20:1903-1911.
218. Hu X-L, Hou G-M, Zhang M-Q, Rong MZ, Ruan WH, Giannelis EP. A new nanocomposite polymer electrolyte based on poly(vinyl alcohol) incorporating hypergrafted nano-silica. *J Mater Chem*. 2012;22:18961-18967.

219. Zhang X, Kar M, Mendes TC, Wu Y, MacFarlane DR. Supported ionic liquid gel membrane electrolytes for flexible supercapacitors. *Adv Energy Mater*. 2018;8:1702702.
220. Sahoo S, Krishnamoorthy K, Pazhamalai P, Mariappan VK, Manoharan S, Kim SJ. High performance self-charging supercapacitors using a porous PVDF-ionic liquid electrolyte sandwiched between two-dimensional graphene electrodes. *J Mater Chem A*. 2019;7:21693-21703.
221. Lai C-C, Lo C-T. Preparation of nanostructural carbon nanofibers and their electrochemical performance for supercapacitors. *Electrochim Acta*. 2015;183:85-93.
222. Ma G, Dong M, Sun K, Feng E, Peng H, Lei Z. A redox mediator doped gel polymer as an electrolyte and separator for a high performance solid state supercapacitor. *J Mater Chem A*. 2015;3:4035-4041.
223. Liu D, Li Q, Zhao H. Electrolyte-assisted hydrothermal synthesis of holey graphene films for all-solid-state supercapacitors. *J Mater Chem A*. 2018;6:11471-11478.
224. Si W, Yan C, Chen Y, Oswald S, Han L, Schmidt OG. On chip, all solid-state and flexible micro-supercapacitors with high performance based on MnO_x/Au multilayers. *Energ Environ Sci*. 2013;6:3218-3223.
225. Wu Z, Jiang L, Tian W, et al. Novel sub-5 nm layered niobium phosphate nanosheets for high-voltage, cation-intercalation typed electrochemical energy storage in wearable pseudocapacitors. *Adv Energy Mater*. 2019;9:1900111.
226. Yang Y, Zhang D, Liu Y, et al. Solid-state double-network hydrogel redox electrolytes for high-performance flexible supercapacitors. *ACS Appl Mater Interfaces*. 2021;13:34168-34177.
227. Veerasubramani GK, Krishnamoorthy K, Pazhamalai P, Kim SJ. Enhanced electrochemical performances of graphene based solid-state flexible cable type supercapacitor using redox mediated polymer gel electrolyte. *Carbon*. 2016;105:638-648.
228. Pan Z, Qiu Y, Yang J, et al. Ultra-endurance flexible all-solid-state asymmetric supercapacitors based on three-dimensionally coated MnO_x nanosheets on nanoporous current collectors. *Nano Energy*. 2016;26:610-619.
229. Wu H, Lou Z, Yang H, Shen G. A flexible spiral-type supercapacitor based on $ZnCo_2O_4$ nanorod electrodes. *Nanoscale*. 2015;7:1921-1926.
230. Fan Y-M, Song W-L, Li X, Fan L-Z. Assembly of graphene aerogels into the 3D biomass-derived carbon frameworks on conductive substrates for flexible supercapacitors. *Carbon*. 2017;111:658-666.
231. Zhi J, Zhao W, Liu X, Chen A, Liu Z, Huang F. Highly conductive ordered mesoporous carbon based electrodes decorated by 3D graphene and 1D silver nanowire for flexible supercapacitor. *Adv Funct Mater*. 2014;24:2013-2019.
232. Su Z, Yang C, Xie B, et al. Scalable fabrication of MnO_2 nanostructure deposited on free-standing Ni nanocone arrays for ultrathin, flexible, high-performance micro-supercapacitor. *Energ Environ Sci*. 2014;7:2652-2659.
233. Zhang L, Zhu P, Zhou F, et al. Flexible asymmetrical solid-state supercapacitors based on laboratory filter paper. *ACS Nano*. 2016;10:1273-1282.
234. Zilong W, Zhu Z, Qiu J, Yang S. High performance flexible solid-state asymmetric supercapacitors from MnO_2/ZnO core-shell nanorods//specially reduced graphene oxide. *J Mater Chem C*. 2014;2:1331-1336.
235. Kang Q, Zhao J, Li X, et al. A single wire as all-inclusive fully functional supercapacitor. *Nano Energy*. 2017;32:201-208.
236. Choi C, Kim KM, Kim KJ, et al. Improvement of system capacitance via weavable superelastic biscrolled yarn supercapacitors. *Nat Commun*. 2016;7:13811.
237. Zhang LL, Zhao XS. Carbon-based materials as supercapacitor electrodes. *Chem Soc Rev*. 2009;38:2520-2531.
238. Chen S, Shi B, He W, et al. Quasifractal networks as current collectors for transparent flexible supercapacitors. *Adv Funct Mater*. 2019;29:1906618.
239. Xue Q, Gan H, Huang Y, et al. Boron element nanowires electrode for supercapacitors. *Adv Energy Mater*. 2018;8:1703117.
240. Gao H, Virya A, Lian K. Proton conducting $H_5BW_{12}O_{40}$ electrolyte for solid supercapacitors. *J Mater Chem A*. 2015;3:21511-21517.
241. Wu P, Cheng S, Yao M, et al. A low-cost, self-standing $NiCo_2O_4$@CNT/CNT multilayer electrode for flexible asymmetric solid-state supercapacitors. *Adv Funct Mater*. 2017;27:1702160.
242. Pal B, Yasin A, Kunwar R, Yang S, Yusoff MM, Jose R. Polymer versus cation of gel polymer electrolytes in the charge storage of asymmetric supercapacitors. *Ind Eng Chem Res*. 2019;58:654-664.
243. Li H, Lv T, Sun H, et al. Ultrastretchable and superior healable supercapacitors based on a double cross-linked hydrogel electrolyte. *Nat Commun*. 2019;10:536.
244. Wolynes PG. Dynamics of electrolyte solutions. *Annu Rev Phys Chem*. 1980;31:345-376.
245. Yuan H, Ma F, Wei X, et al. Ionic-conducting and robust multilayered solid electrolyte interphases for greatly improved rate and cycling capabilities of sodium ion full cells. *Adv Energy Mater*. 2020;10:2001418.
246. Nguyen CA, Argun AA, Hammond PT, Lu X, Lee PS. Layer-by-layer assembled solid polymer electrolyte for electrochromic devices. *Chem Mater*. 2011;23:2142-2149.
247. Park J, Kim B, Yoo Y-E, Chung H, Kim W. Energy-density enhancement of carbon-nanotube-based supercapacitors with redox couple in organic electrolyte. *ACS Appl Mater Interfaces*. 2014;6:19499-19503.
248. Kötz R, Hahn M, Ruch P, Gallay R. Comparison of pressure evolution in supercapacitor devices using different aprotic solvents. *Electrochem Commun*. 2008;10:359-362.
249. Ramasamy C, Palma del vel J, Anderson M. An activated carbon supercapacitor analysis by using a gel electrolyte of sodium salt-polyethylene oxide in an organic mixture solvent. *J Solid State Electr*. 2014;18:2217-2223.
250. Cai J, Wang Y, Qiao X, Zhou X, Mansour AN. A novel mediator-containing polyvinylidene fluoride/lithium trifluoromethanesulfonate polymer electrolyte membrane for low-temperature solid-state supercapacitors. *Mater Lett*. 2019;251:26-29.
251. Bahuguna G, Ram P, Sharma RK, Gupta R. An organofluorine compound mixed electrolyte for ultrafast electric double layer supercapacitors. *ChemElectroChem*. 2018;5:2767-2773.

252. Lé T, Aradilla D, Bidan G, et al. Unveiling the ionic exchange mechanisms in vertically-oriented graphene nanosheet supercapacitor electrodes with electrochemical quartz crystal microbalance and ac-electrogravimetry. *Electrochem Commun*. 2018;93:5-9.
253. Xu J, Yang N, Heuser S, et al. Achieving ultrahigh energy densities of supercapacitors with porous titanium carbide/boron-doped diamond composite electrodes. *Adv Energy Mater*. 2019;9:1803623.
254. McAllister BT, Schon TB, DiCarmine PM, Seferos DS. A study of fused-ring thieno[3,4-e]pyrazine polymers as n-type materials for organic supercapacitors. *Polym Chem*. 2017;8:5194-5202.
255. Guo Y, Li W, Yu H, Perepichka DF, Meng H. Flexible asymmetric supercapacitors via spray coating of a new electrochromic donor-acceptor polymer. *Adv Energy Mater*. 2017;7:1601623.
256. Lé T, Gentile P, Bidan G, Aradilla D. New electrolyte mixture of propylene carbonate and butyltrimethylammonium bis (trifluoromethylsulfonyl)imide (N1114 TFSI) for high performance silicon nanowire (SiNW)-based supercapacitor applications. *Electrochim Acta*. 2017;254:368-374.
257. Béguin F, Frąckowiak E. *Supercapacitors: Materials, Systems, and Applications*. John Wiley & Sons; 2013.
258. Salunkhe RR, Young C, Tang J, et al. A high-performance supercapacitor cell based on ZIF-8-derived nanoporous carbon using an organic electrolyte. *Chem Commun*. 2016;52:13620.
259. Sato T, Masuda G, Takagi K. Electrochemical properties of novel ionic liquids for electric double layer capacitor applications. *Electrochim Acta*. 2004;49:3603-3611.
260. Armand M, Endres F, MacFarlane DR, Ohno H, Scrosati B. Ionic-liquid materials for the electrochemical challenges of the future. *Nat Mater*. 2009;8:621-629.
261. Zhang S, Sun N, He X, Lu X, Zhang X. Physical properties of ionic liquids: database and evaluation. *J Phys Chem Ref Data*. 2006;35:1475-1517.
262. Schon TB, DiCarmine PM, Seferos DS. Polyfullerene electrodes for high power supercapacitors. *Adv Energy Mater*. 2014;4:1301509.
263. Anouti M, Timperman L, El hilali M, Boisset A, Galiano H. Sulfonium bis(trifluorosulfonimide) plastic crystal ionic liquid as an electrolyte at elevated temperature for high-energy supercapacitors. *J Phys Chem C*. 2012;116:9412-9418.
264. Rennie AJR, Martins VL, Torresi RM, Hall PJ. Ionic liquids containing sulfonium cations as electrolytes for electrochemical double layer capacitors. *J Phys Chem C*. 2015;119:23865-23874.
265. Suleman M, Othman MAR, Hashmi SA, et al. Activated graphene oxide/reduced graphene oxide electrodes and low viscous sulfonium cation based ionic liquid incorporated flexible gel polymer electrolyte for high rate supercapacitors. *J Alloy Compd*. 2017;695:3376-3392.
266. Pan Z, Yang J, Zhang Q, et al. All-solid-state fiber supercapacitors with ultrahigh volumetric energy density and outstanding flexibility. *Adv Energy Mater*. 2019;9:1802753.
267. Tamilarasan P, Ramaprabhu S. Graphene based all-solid-state supercapacitors with ionic liquid incorporated polyacrylonitrile electrolyte. *Energy*. 2013;51:374-381.
268. Zhang X, Wang L, Peng J, et al. A flexible ionic liquid gelled PVA-Li_2SO_4 polymer electrolyte for semi-solid-state supercapacitors. *Adv Mater Interfaces*. 2015;2:1500267.
269. Ayalneh TG, Muñoz-Torrero D, Palma J, Anderson M, Marcilla R. All-solid state supercapacitors operating at 3.5 V by using ionic liquid based polymer electrolytes. *J Power Sources*. 2015;279:472-480.
270. Tiruye GA, Muñoz-Torrero D, Palma J, Anderson M, Marcilla R. Performance of solid state supercapacitors based on polymer electrolytes containing different ionic liquids. *J Power Sources*. 2016;326:560-568.
271. Elamin K, Shojaatalhosseini M, Danyliv O, Martinelli A, Swenson J. Conduction mechanism in polymeric membranes based on PEO or PVdF-HFP and containing a piperidinium ionic liquid. *Electrochim Acta*. 2019;299:979-986.
272. Chapman Varela J, Sankar K, Hino A, et al. Piperidinium ionic liquids as electrolyte solvents for sustained high temperature supercapacitor operation. *Chem Commun*. 2018;54:5590-5593.
273. Zhang S, Brahim S, Maat S. High-voltage operation of binder-free CNT supercapacitors using ionic liquid electrolytes. *J Mater Res*. 2018;33:1179-1188.
274. Ruan D, Zuo F. High voltage performance of spiro-type quaternary ammonium salt based electrolytes in commercial large supercapacitors. *Electrochemistry*. 2015;83:997-999.
275. Shi X, Zhang W, Wang J, et al. $(EMIm)^+(PF6)^-$ ionic liquid unlocks optimum energy/power density for architecture of nanocarbon-based dual-ion battery. *Adv Energy Mater*. 2016;6:1601378.
276. Osti NC, Gallegos A, Dyatkin B, Wu J, Gogotsi Y, Mamontov E. Mixed ionic liquid improves electrolyte dynamics in supercapacitors. *J Phys Chem C*. 2018;122:10476-10481.
277. Siyahjani S, Oner S, Singh PK, Varlikli C. Highly efficient supercapacitor using single-walled carbon nanotube electrodes and ionic liquid incorporated solid gel electrolyte. *High Perform Polym*. 2018;30:971-977.
278. Borenstein A, Attias R, Hanna O, Luski S, Kaner RB, Aurbach D. A surprising failure mechanism in symmetric supercapacitors at high voltages. *ChemElectroChem*. 2017;4:2660-2668.
279. Hou Y, Chen L, Hirata A, Fujita T, Chen M. Non-aqueous nanoporous gold based supercapacitors with high specific energy. *Scripta Mater*. 2016;116:76-81.
280. Huang P-L, Luo X-F, Peng Y-Y, et al. Ionic liquid electrolytes with various constituent ions for graphene-based supercapacitors. *Electrochim Acta*. 2015;161:371-377.
281. Galiński M, Lewandowski A, Stępniak I. Ionic liquids as electrolytes. *Electrochim Acta*. 2006;51:5567-5580.
282. Yang X, Zhang L, Zhang F, Zhang T, Huang Y, Chen Y. A high-performance all-solid-state supercapacitor with graphene-doped carbon material electrodes and a graphene oxide-doped ion gel electrolyte. *Carbon*. 2014;72:381-386.
283. She Z, Ghosh D, Pope MA. Decorating graphene oxide with ionic liquid nanodroplets: an approach leading to energy-dense, high-voltage supercapacitors. *ACS Nano*. 2017;11:10077-10087.
284. Pandey GP, Hashmi SA. Ionic liquid 1-ethyl-3-methylimidazolium tetracyanoborate-based gel polymer electrolyte for electrochemical capacitors. *J Mater Chem A*. 2013;1:3372-3378.

285. Lin R, Taberna P-L, Fantini S, et al. Capacitive energy storage from −50 to 100 °C using an ionic liquid electrolyte. *J Phys Chem Lett*. 2011;2:2396-2401.
286. Shen B, Guo R, Lang J, Liu L, Liu L, Yan X. A high-temperature flexible supercapacitor based on pseudocapacitive behavior of FeOOH in an ionic liquid electrolyte. *J Mater Chem A*. 2016;4:8316-8327.
287. Yang Y, Zhu T, Chi C, Liu L, Zheng J, Gong X. All-solid-state asymmetric supercapacitors with novel ionic liquid gel electrolytes. *ACS Appl Electron Mater*. 2020;2:3906-3914.
288. Wang K, Zhang X, Li C, et al. Chemically crosslinked hydrogel film leads to integrated flexible supercapacitors with superior performance. *Adv Mater*. 2015;27:7451-7457.
289. Yang Y, Huang Q, Niu L, et al. Waterproof, ultrahigh areal-capacitance, wearable supercapacitor fabrics. *Adv Mater*. 2017;29:1606679.
290. Ye T, Li L, Zhang Y. Recent progress in solid electrolytes for energy storage devices. *Adv Funct Mater*. 2020;30:2000077.
291. Lin T, Shi M, Huang F, et al. One-pot synthesis of a double-network hydrogel electrolyte with extraordinarily excellent mechanical properties for a highly compressible and bendable flexible supercapacitor. *ACS Appl Mater Interfaces*. 2018;10:29684-29693.
292. Wang Y, Chen F, Liu Z, et al. A highly elastic and reversibly stretchable all-polymer supercapacitor. *Angew Chem Int Ed*. 2019;58:15707-15711.
293. Zhang H, Niu W, Zhang S. Extremely stretchable, sticky and conductive double-network ionic hydrogel for ultra-stretchable and compressible supercapacitors. *Chem Eng J*. 2020;387:124105.
294. Liu Y, Lu N, Liu F, et al. Highly strong and tough double-crosslinked hydrogel electrolyte for flexible supercapacitors. *ChemElectroChem*. 2020;7:1007-1015.
295. Li W, Gao F, Wang X, Zhang N, Ma M. Strong and robust polyaniline-based supramolecular hydrogels for flexible supercapacitors. *Angew Chem Int Ed*. 2016;55:9196-9201.
296. Huang J, Peng S, Gu J, et al. Self-powered integrated system of a strain sensor and flexible all-solid-state supercapacitor by using a high performance ionic organohydrogel. *Mater Horiz*. 2020;7:2085-2096.
297. Zhang D, Liu Y, Liu Y, et al. A general crosslinker strategy to realize intrinsic frozen resistance of hydrogels. *Adv Mater*. 2021;33:2104006.
298. Zhang D, Tang Y, Zhang Y, et al. Highly stretchable, self-adhesive, biocompatible, conductive hydrogels as fully polymeric strain sensors. *J Mater Chem A*. 2020;8:20474-20485.
299. Tang Z, He H, Zhu L, et al. A general protein unfolding-chemical coupling strategy for pure protein hydrogels with mechanically strong and multifunctional properties. *Adv Sci*. 2021;9:2102557.
300. Xu D, Hu W, Sun XN, Cui P, Chen XY. Redox additives of Na_2MoO_4 and KI: synergistic effect and the improved capacitive performances for carbon-based supercapacitors. *J Power Sources*. 2017;341:448-456.

AUTHOR BIOGRAPHIES

Yongrui Yang received his Master degree under the supervision of Prof. Xiong Gong in the School of Polymer Science and Polymer Engineering at the University of Akron (USA) in 2020. Now he is a PhD candidate in the Institute of Chemistry at Chinese Academy of Sciences (ICCAS). His research interest includes flexible supercapacitors, novel electrolyte materials, and transparent electrodes.

Prof. Xiong Gong is a full professor in the School of Polymer Science and Polymer Engineering at the University of Akron (USA). Dr. Gong holds a secondary position as a full professor in the Department of Chemical, Biomolecular and Corrosion Engineering at USA. Prior to Akron, he was a manager of advanced materials and devices at CBrite Inc. and a senior research scientist at the University of California at Santa Barbara, working with Prof. Alan J. Heeger (the Nobel Prize in Chemistry 2000). Currently, his current research focuses on organic and hybrid inorganic-organic perovskite electronic materials and electronics, thermoelectric materials and devices, solid-state flexible supercapacitors. So far, he authored and co-authored over 240 peer-reviewed articles, with over 26,000 peer-citation. He earned an H-index of 70. He also contributed 9 book chapters and 35 granted and pending patents.

How to cite this article: Yang Y, Zhu T, Shen L, et al. Recent progress in the all-solid-state flexible supercapacitors. *SmartMat*. 2022;1-35. doi:10.1002/smm2.1103